Characterisation of a novel component of a nuclear calcium channel in plant symbioses

Janni Seppä

Thesis submitted for the degree of

MSc by Research

to the

University of East Anglia

Research conducted at the John Innes Centre

September 2023

This copy of the thesis has been supplied on condition that anyone who consults it is understood to recognise that its copyright rests with the author and that use of any information derived therefrom must be in accordance with current UK Copyright Law. In addition, any quotation or extract must include full attribution.

Abstract

Mutualistic associations with soil microbes can improve plant nutrition by improving access to difficult-to-obtain nutrients such as nitrates and phosphorus. The establishment of both rhizobial and arbuscular mycorrhizal symbioses requires the activation of calcium oscillations after the perception of elicitors from the symbionts by plasma membrane receptors. The calcium oscillation starts inside the nucleus and the release of calcium from a store between the nuclear membranes is orchestrated by two nuclear-localised ion channels: a cation channel (DMI1), and a calcium channel composed of the subunit proteins Cyclic Nucleotide Gated Channel (CNGC) 15a, b and c. CNGCs are known to form tetrameric complexes, raising the question of the stoichiometry of the CNGC15a, b, c channel complex in the nuclear envelope. CNGCD, another member of the CNGC family in *Medicago truncatula*, was recently identified as a putative interactor with CNGC15a. CNGCD may therefore form a heterotetrameric complex with CNGC15a, b and c. Here I aim to characterise the function of CNGCD in symbioses using expression analysis, interaction assays and CRISPR-Cas9. I find that *CNGCD* is expressed in symbiotic tissues and can interact with other components of the nuclear calcium signalling machinery. Biallelic knockout of *cngcD* in *M. truncatula* hairy roots leads to a loss of nodulation. Taken together, I demonstrate that CNGCD can form a complex with CNGC15a, b, c and has a role in root nodule symbiosis.

Access Condition and Agreement

Each deposit in UEA Digital Repository is protected by copyright and other intellectual property rights, and duplication or sale of all or part of any of the Data Collections is not permitted, except that material may be duplicated by you for your research use or for educational purposes in electronic or print form. You must obtain permission from the copyright holder, usually the author, for any other use. Exceptions only apply where a deposit may be explicitly provided under a stated licence, such as a Creative Commons licence or Open Government licence.

Electronic or print copies may not be offered, whether for sale or otherwise to anyone, unless explicitly stated under a Creative Commons or Open Government license. Unauthorised reproduction, editing or reformatting for resale purposes is explicitly prohibited (except where approved by the copyright holder themselves) and UEA reserves the right to take immediate ‘take down’ action on behalf of the copyright and/or rights holder if this Access condition of the UEA Digital Repository is breached. Any material in this database has been supplied on the understanding that it is copyright material and that no quotation from the material may be published without proper acknowledgement.

Table of Contents

Abstract *2*

List of Figures *4*

Acknowledgements *5*

1. Introduction *6*

1.1. Ca^{2+} as a ubiquitous secondary messenger **6**

1.1.1. Cyclic nucleotide-gated channels in plants and animals 7

1.2. Plant root endosymbioses **9**

1.2.1. Common symbiosis signalling pathway 10

1.3. Background and specific objectives **12**

2. Results *14*

2.1. Expression of *pCNGC15:GUS* and *pCNGCD:GUS* in symbiotic tissues **14**

2.2. Pairwise interaction between CNGCD and components of the symbiotic calcium channel complex **16**

2.3. Phenotyping of *cngcD* mutants **21**

2.3.1. Phenotyping of *cngcD* EMS mutant lines 21

2.3.2. CRISPR-Cas9 of *cngcD* in hairy roots 23

2.3.2. Generation of *cngcD*-CRISPRCas9 stable lines 26

3. Discussion *28*

4. Materials and Methods *34*

5. References *40*

6. Appendix *47*

Appendix 1. List of constructs used. **47**

Appendix 2. List of primers used. **50**

List of Figures

Figure 1. *Promoter:GUS* expression analysis of *CNGCD* and *CNGC15s* in symbiotic tissue.

Figure 2. Pairwise interaction between CNGCD and CNGC15s and DMI1 by bimolecular fluorescence complementation.

Figure 3. Self pairwise interaction of CNGC15s and CNGCD by bimolecular fluorescence complementation.

Figure 4. Western blot of bimolecular fluorescence complementation (biFC) fusion proteins (Figs 2&3).

Figure 5. CNGCD N-terminus interaction with DMI1 C-terminus in pairwise GAL4-based yeast two-hybrid system.

Figure 6. Nodulation (A) and mycorrhizal colonisation (B) in backcrossed EMS mutant *cngcD* x YC3.6 lines.

Figure 7. Nodulation in hairy roots expressing *Cas9* and gRNAs targeting *CNGCD*.

Acknowledgements

The constructs for promoter:GUS (Fig. 1) were made by Nicola Cook and Myriam Charpentier, for biFC (Figs 2-4) by Rik Huisman and Myriam Charpentier, for yeast two-hybrid (Fig 5) by Myriam Charpentier and Pablo Del Cerro Sánchez, for CNGCD-CRISPR (Fig. 7) by Rik Huisman and by Nicola Cook for stable transformation of CNGCD-CRISPR. Preliminary work for this project was performed by Rik Huisman (IP-MS and biFC in *N. benthamiana*) and Giulia Gobbato (initial phenotyping of EMS lines, promoter:GUS).

Thank you to Myriam for her excellent advice and for always challenging me to be a better scientist. My warm thanks to my secondary supervisor, Phil Carella, for his helpful perspectives on my work. Thank you to Charpentier group members, past and present, for their support and advice: Edmund Bridge, Nicola Cook, Pierre Dangeville, Pablo Del Cerro Sánchez, Giulia Gobbato, Lauren Grubb, Catherine Jacott, Anson Lam, Clémence Rodney, Emily Tipper, and Shouchao Yan.

Thank you to Thomas Navarro Sens and George Seddon-Roberts for chats in the hallway, lunches, dinners and company during mandatory training.

Finally, thank you to my wonderful best friends Brodie, Foley, Liz and Nat, for always looking after me, and to Sean, for unflinching support during difficult times (and the easy ones).

1. Introduction

1.1. Ca^{2+} as a ubiquitous secondary messenger

Cells respond to changes in their environment through signal transduction. In plant and animal cells, free calcium ions (Ca^{2+}) act as a second messenger, with changes in Ca^{2+} concentration, typically in the cytosol, effecting downstream processes in signalling cascades. In plants, rapid, transient Ca^{2+} influxes are observed in response to many abiotic and biotic stimuli.

In a resting cell, cytosolic Ca^{2+} concentration is maintained at 50-100nM, and on recognition of an extracellular signal, can increase to low-µM levels (Edel et al., 2017; Demidchik et al., 2018). The Ca^{2+} concentration in the cell wall and in intracellular calcium stores, such as the ER and vacuole, is typically much higher (0.1–10 mM), and Ca^{2+} signals can therefore be generated by passive release of Ca^{2+} down the electrochemical gradient, through calcium-permeable channels (Demidchik et al., 2018). Sustained increases in cytosolic Ca^{2+} concentration to above 100µM are cytotoxic, so a low intracellular concentration is maintained through transport and buffering, and Ca^{2+} release from Ca^{2+} stores is carefully controlled through the regulation of Ca^{2+}-permeable channels and rapid efflux on generation of a calcium signal (Edel et al., 2017; Demidchik et al., 2018).

The ubiquity of changes in cytosolic Ca^{2+} concentration as a second messenger raises the question of how a common second messenger can maintain specificity when decoded by a downstream signalling element. Several mechanisms may contribute to maintaining a Ca^{2+} signal's specificity, including: subcellular location of the Ca^{2+} release, requirement for synchronised signalling events, and expression of specific signalling machinery in different cell types (McAinsh and Pittman, 2009). Organelles, including chloroplasts and nuclei, are capable of generating calcium signals (Charpentier, 2018; Kelner et al., 2018; Lenzoni and Knight, 2019). Transient calcium spikes and waves or oscillations show observable stimulus-specific temporal dynamics – magnitude, wavelength, number, and frequency – known as the calcium signature. This has led to the hypothesis that the specificity of a Ca^{2+} signal is encoded by the temporal dynamics of the Ca^{2+} release itself (McAinsh and Pittman, 2009).

Rapid release of Ca^{2+} into the cytoplasm or organelles occurs passively through calcium-permeable cation channels (Demidchik et al., 2018). Compared with animals and algae, plants have lost several Ca^{2+} influx mechanisms during evolution, including several canonical Ca^{2+} channels; hence ion channels controlling calcium influx are generally referred to as 'calcium-permeable channels', permeable to several cations rather than calcium-specific (Edel et al., 2017; Demidchik et al., 2018). The groups of calcium-permeable channels present in plants include cyclic nucleotide-gated channels (CNGCs), ionotropic glutamate receptors (GLRs), mechanosensitive-like channels (MSLs), Mid1-complementing activity channels (MCA) and reduced hyperosmolarity-induced $[Ca^{2+}]_{cyt}$ increase channels (OSCAs) (Demidchik et al., 2018).

1.1.1. Cyclic nucleotide-gated channels in plants and animals

Cyclic nucleotide-gated channels (CNGCs) belong to the voltage-gated ion channel superfamily, and like other members of this superfamily, form tetrameric complexes, with each subunit containing six transmembrane domains and cytosolic N- and C-terminal domains (Dietrich et al., 2020). The C-terminus contains cyclic nucleotide binding domains (CNBD) and calmodulin-binding domains (CaMBD). The *Arabidopsis* CNGC family has 20 members, forming five clades (I, II, III, IVa and IVb) (Mäser et al., 2001). Plant CNGCs are homologous to the cyclic nucleotide-gated (CNG) and hyperpolarisation-activated cyclic nucleotide gated (HCN) channels in animals, which have similar structure and domain organisation. These channels have roles in visual perception, olfaction and heart and central nervous system functioning, and therefore implicated in several human diseases (Biel, 2009).

Early findings suggested that CNGCs are nonselective ion channels, but more recently several plant CNGCs have been found to be permeable to Ca^{2+} but not K^+ (Meena et al., 2019; Pan et al., 2019). Early electrophysiological characterisations of CNGCs in *Xenopus laevis* oocytes found activation by cAMP and cGMP (Leng et al., 1999, 2002; Balagué et al., 2003). More recent studies have found CNGC activation without requirement for cyclic nucleotides: AtCNGC11/12 do not require cAMP or cGMP for activity (Zhang et al., 2019). On recognition of bacterial flagellin, the AtCNGC2/4 heterocomplex in *Arabidopsis* is activated by BIK1 without requirement for cyclic nucleotides (Tian et al., 2019).

Cyclic nucleotides bind CNGCs in the C-terminal CNBD, which overlaps with a CaMBD. Overlap between CNBDs and CaMBDs led to the hypothesis that cyclic nucleotides and CaMs competitively bind CNGCs to activate or close the channel (Arazi et al., 2000). CaM7 negatively regulates AtCNGC14-mediated signalling in root hair growth (Zeb et al., 2020). In symbiotic calcium oscillations, calcium loaded CaM2 binds to the C-terminus IQ domain of MtCNGC15s to close the channel (del Cerro et al., 2022). In AtCNGC12, CaMs can bind additional motifs in the N- and C-terminal domains, with CaM binding having both positive and negative regulatory roles (DeFalco et al., 2016). AtCNGC12 activity is enhanced when bound to CaM1 in *X. laevis* oocytes (Zhang et al., 2019).

Plant CNGCs can form heterotetramers with specific functions. Heterotetramerisation may allow for specific calcium signals, since each subunit will have unique interaction partners and generate a calcium channel with specific gating and ion permeability. In *Arabidopsis*, CNGC heterotetramers are implicated in a number of processes, as implicated by phenotype and interaction assays: CNGC2/4/6 in immunity and thermosensing, CNGC2/4 in floral growth, CNGC18/7/8 in regulation of pollen tube growth, CNGC6/9/14 in root hair growth, CNGC5/6/9/12 in ABA-induced stomatal closure, and CNGC15a, b and c in root endosymbioses (Chin et al., 2013; Charpentier et al., 2016; Brost et al., 2019; Pan et al., 2019; Tian et al., 2019; Ma et al., 2023; Tan et al., 2023). However, it is currently unknown what stoichiometries heterotetrameric CNGC complexes form *in planta*, given that CNGC subunits can form calcium-permeable homotetramers in heterologous systems like *X. laevis* oocytes (Charpentier et al., 2016; Pan et al., 2019).

In contrast, there is extensive structural information from cryo-EM and x-ray crystallography on homologous channels in animals. In rod and cone cells, CNG channels form heterotetramers with a 3A:1B stoichiometry, with three CNGA1 or CNGA3 and one CNGA2 or CNGA4 subunit per channel (Weitz et al., 2002; Ding et al., 2012). Stoichiometry is maintained through interaction between the C-terminal leucine zipper domains in the CNGA1/A3 subunits (Zhong et al., 2002; Shuart et al., 2011; Xue et al., 2022). There are also resolved structures of human HCN1 channels, C. elegans TAX-4 and prokaryotic LliK (James et al., 2017; Lee and MacKinnon, 2017; Li et al., 2017). Since C-terminal domains in plant CNGCs have diverged from

animal and prokaryotic homologues, more detailed structural information on plant CNGCs is required to understand complex formation and inter-subunit interaction.

1.2. Plant root endosymbioses

Plants encounter myriad microorganisms in the soil: pathogenic, neutral, and beneficial. Associations with beneficial microbes, in long-term mutualistic symbioses or the maintenance of the root microbiome, incur benefits including improved defence against pathogens and herbivores, resistance to abiotic stress, and access to nutrients. Most flowering plants (around 80%) associate with arbuscular mycorrhizal fungi (AMF), including important crop species like wheat and rice (Harrison, 2005). Species in four families in the rosid clade associate with nitrogen-fixing rhizobial bacteria: Fabales, Rosales, Fagales and Curcubitales, known together as the nitrogen-fixing clade, though not all species in the clade form associations with nitrogen-fixing bacteria (Soltis et al., 1995). The most notable examples of nitrogen-fixing plants are legumes, including important crops such as soybean, peas, and the forage crop alfalfa. Legumes are particularly efficient at nitrogen fixation and are of special research interest due to their decreased need for nitrogen fertilisers, their use in improving soil quality and crop nitrogen content when rotated with non-legume crops, and their high protein content (Foyer et al., 2016). Together, root mutualisms with rhizobia and AMF may be referred to as endosymbioses, since both require accommodation of the symbiont within the host cell, and both processes have notable signalling events in common.

The nodule, the root organ produced by association with rhizobia, and the arbuscule, an intracellular fungal structure in contact with host membranes, are primarily sites of nutrient exchange. Rhizobial bacteroids in the nodule fix atmospheric nitrogen into forms that can be used for plant metabolism (Oldroyd et al., 2011). AM fungi provide plants with difficult-to-obtain nutrients, in particular, phosphorus and nitrogen (Ames et al., 1983; Govindarajulu et al., 2005; Harrison, 2005). The symbionts, in return, receive carbon from the host plant. Symbioses with AM fungi also make plants more resistant to pathogens and abiotic stress (Miransari, 2010).

Rhizobial infection begins when rhizobia are detected at the surfaces of root hairs within the infection zone – distal of the root meristem – leading to root hair curling around attached rhizobia. Rhizobia grow down the length of the root hair, in a structure

called an infection thread, and into the root epidermis. Simultaneous signalling in the cortex leads to cell division and the start of nodule organogenesis, controlled primarily by auxin and cytokinin signalling (Oldroyd et al., 2011). The mature nodule contains both host- and symbiont-derived cells. The rhizobia terminally differentiate within the nodule, from free-living bacteria to bacteroids contained in host cells. Bacterial nitrogenases catalyse nitrogen fixation, and host-derived leghemoglobins buffer oxygen in the mature nodule, as free O_2 deactivates nitrogenase. Legume nodules are described as either determinate or indeterminate, based on loss or retention of the nodule meristem. Species forming determinate nodules include *Glycine max*, *Phaseolus* spp. and *Lotus japonicus*, while *Medicago truncatula* and *Pisum* spp. form indeterminate nodules.

AM fungi are obligate biotrophs belonging to the phylum Glomeromycotina (Harrison, 2005). Fungal spores living in the soil, attracted to strigolactones produced by the host, produce a hyphal germ tube that searches the soil for the host root (Harrison, 1997). The hypha differentiates to form an appressorium, which penetrates the host root epidermis (Harrison, 1997). The fungus grows in the root cortex, with branching hyphae in the inner cortex developing into branched, terminal hyphae called arbuscules (Harrison, 1997). The arbuscule is surrounded by host membrane despite growing within the cortical cells, with a large surface area between host and fungus for nutrient exchange (Harrison, 1997). The fungae also produce thick-walled lipid storage vesicles within and between cells (Choi et al., 2018).

1.2.1. Common symbiosis signalling pathway

Plants secrete flavonoids and strigolactones, which are recognised by rhizobia and AMF respectively. In response, the microbes secrete rhizobial Nod or fungal Myc factors, made of chitin derivatives, that are recognised at the host cell surface. Recognition of both Nod and Myc factors at the cell surface leads to shared early signalling events, known as the common symbiosis signalling pathway.

Nod lipochitooligosaccharides (Nod-LCOs) are thought to mediate host-mutualist specificity in legume-rhizobia interactions, since their composition varies widely among species of rhizobia (Liang et al., 2014). In *M. truncatula* Nod-LCOs are recognised by lysine motif receptor-like kinases (LysM-RLK) Nod Factor Perception

(NFP) and LysM-containing receptor kinase (LYK) 3 (Nod Factor Receptor 5 (NFR5) and NFR1 in *L. japonicus*) and Myc chito-oligosaccharides (Cos) are recognised by Myc Factor Receptor 1 (MYR1) and Chitin Elicitor Receptor Kinase 1 (CERK1) in rice, with other LysM receptors likely involved in Myc LCO and CO recognition (Zhang et al., 2015; He et al., 2019). Does Not Make Infections 2 (DMI2) (Symbiosis Receptor Kinase or SYMRK in *L. japonicus*), a RLK downstream of NFP and LYK3, is also involved in common signalling pathways (Endre et al., 2002; Stracke et al., 2002).

A central component of early symbiotic signalling is the generation of a nuclear calcium oscillation. This calcium oscillation is required for both rhizobial and AM symbioses. The signal is transduced from the plasma membrane to the nuclear envelope by an unknown mechanism, though the mevalonate pathway has been implicated in inducing downstream signalling events, and G-protein signalling may be required for root nodule symbiosis (Kevei et al., 2007; Choudhury and Pandey, 2013, 2015; Venkateshwaran et al., 2015). Three membrane proteins, localised to the nuclear envelope, are required to generate the nuclear Ca^{2+} oscillation: MCA8, a type IIA SERCA ATPase, DMI1, a nonselective cation channel, and CNGC15a/b/c, a calcium channel (Capoen et al., 2011; Charpentier et al., 2016). DMI1 and CNGC15 interact and are predicted to allow simultaneous movement of ions (Charpentier et al., 2016). DMI1 is thought to act as a counter-ion channel, allowing movement of potassium ions into the nuclear lumen, triggering the influx of calcium into the nucleoplasm via CNGC15. Ca^{2+}-bound CaM2 binds CNGC15s to close the calcium channel (del Cerro et al., 2022). Rhizobia and AM fungi induce calcium oscillations with similar signatures in the epidermis and cortex (Sieberer et al., 2012). In outer cortical cells, slow frequency Ca^{2+} oscillations precede microbial entry into the cortical cell layer, and high-frequency oscillations begin when the symbiont makes contact with the cortical cell layer (Sieberer et al., 2012).

The calcium oscillation is decoded by a calcium-/calmodulin-dependent kinase (CCaMK; called DMI3 in *M. truncatula*), which forms a complex with the transcription factor Interacting Partner of DMI3 (IPD3; CYCLOPS in *L. japonicus*) to regulate transcription of target genes. In addition to IPD3, a number of other transcription factors have roles in both AM and RN symbioses, including the gibberellic acid signalling repressors and GRAS-type transcription factors, DELLAs (Floss et al., 2013;

Fonouni-Farde et al., 2016; Jin et al., 2016). Nodulation Signalling Pathway 1&2 (NSP1/2), GRAS transcription factors originally identified for their role in nodulation, also appear to be important for mycorrhization (Hirsch and Oldroyd, 2009; MacLean et al., 2017).

Though there is convergence at early signalling events, clearly there are divergent outputs from Nod and Myc factor signalling, leading to the formation of nodules and arbusculation of root cells respectively. A minority of the transcriptional programs activated by rhizobia and AMF are shared, though shared early signalling components are required for transcription of RNS- or AM-specific genes. Specificity is maintained from Nod and Myc factor recognition, though there is convergence at the nuclear calcium oscillation, so it is possible that multiple pathways run concurrently, or that common symbiosis genes are specifically regulated throughout. Recent transcriptomic studies have shown that extensive transcriptional reprogramming occurs in both symbioses in a specific manner, with a small percentage of shared early signalling (Manthey et al., 2004; Hohnjec et al., 2005; Deguchi et al., 2007; Tromas et al., 2012; Nanjareddy et al., 2017; Sakamoto et al., 2019).

1.3. Background and specific objectives

A fourth putative component of the symbiotic nuclear calcium channel, CNGCD, was identified as a strong interactor with CNGC15a via immunoprecipitation followed by mass-spectrophotometry (IP-MS) (Charpentier lab, unpublished data). CNGCD interacts with CNGC15s, itself and DMI1 in biFC assays in *Nicotiana benthamiana* (Charpentier lab, unpublished data). Given that CNGCD interacts with CNGC15s and DMI1 in *Nicotiana benthamiana*, it may form a heterotetrameric complex with CNGC15s in *M. truncatula* root cells. My aim was to further characterise CNGCD and its role in symbioses.

My specific objectives were:

1. To characterise the *CNGCD* expression pattern in symbiotic tissues (nodules and AMF-colonised roots) using a *pCNGCD:GUS* construct.
2. To demonstrate if CNGCD could interact with itself and other components of the nuclear calcium signalling machinery in *M. truncatula*.

3. Characterise the phenotype of *cngcD* and identify a stable mutant line.

2. Results

2.1. Expression of *pCNGC15:GUS* and *pCNGCD:GUS* in symbiotic tissues

To assess whether *CNGCD* has a similar expression pattern as *CNGC15a, CNGC15b* and *CNGC15c*, the *CNGCD* promoter was fused to the bacterial *β-Glucuronidase* (*GUS*) *(pCNGCD:GUS)* in the PKGW-RR-GUS vector. *pCNGCD:GUS* as well as *pCNGC15a:GUS, pCNGC15b:GUS* and *pCNGC15c:GUS* were expressed in R108 *M. truncatula* roots via *Agrobacterium rhizogenes*-mediated transformation (Chabaud et al., 2006). 28 days post-inoculation (dpi) with *Sinorhizobium meliloti* 2011 (*Sm*2011) the nodules were collected, and *GUS* expression was assessed (Fig.1a). 2mM X-gluc was vacuum-infiltrated into the nodules to create blue staining where the GUS enzyme is expressed. The expression of *GUS* driven by promoters of *CNGC15a, CNGC15b, CNGC15c* or *CNGCD* was detected in the apical regions of the nodules (Fig. 1a). Sectioning of additional nodules confirmed that each *CNGC* was expressed in the nodule apex (Fig. 1a). *pCNGC15a:GUS, pCNGC15b:GUS* and *pCNGC15c:GUS* expression were concentrated in the meristem and epidermis, whereas *GUS* expression driven by *CNGCD* promoter was more diffuse through the nodule (Fig.1a). Transformed roots inoculated with AM fungi 8 weeks post-inoculation (wpi) showed *pCNGCD:GUS* expression through all cell layers included cortical cells colonised with AM (Fig. 1b). This is similar to the expression of *CNGC15a, CNGC15b* and *CNGC15c* (Charpentier lab, unpublished data). Taken together, these results demonstrate that *CNGCD* is expressed in symbiotic tissues and may therefore have a function in symbioses.

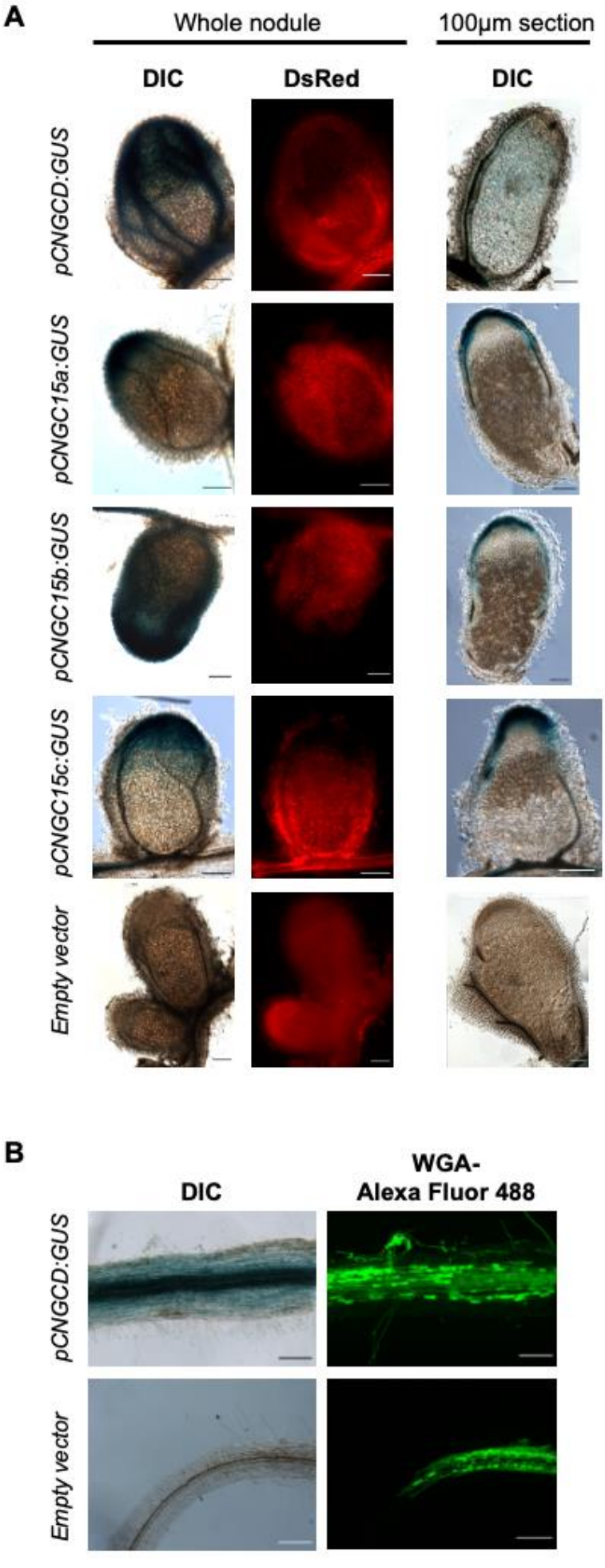


Figure 1. *Promoter:GUS* expression analysis of *CNGCD* and *CNGC15s* in symbiotic tissue. Wild-type R108 *M. truncatula* hairy roots expressing the native promoter of each *CNGC* fused to *β-Glucuronidase* were inoculated with *Sinorhizobium meliloti* 2011 (*Sm*2011) (A) and *Rhizophagus irregularis* (B). *DsRed* was used as a transformation marker. Empty vector contains *GUS* without a promoter. All scale bars represent 200µm. (A) Expression of *CNGCD* and *CNGC15s* in whole nodules (first and second column) and 100µm sections of nodules. Nodules were imaged at 28 dpi. (B) Expression of *CNGCD* in arbuscule-containing cortical cells 8 wpi. Roots were stained with WGA-Alexa Fluor 488 to visualise fungal structures.

2.2. Pairwise interaction between CNGCD and components of the symbiotic calcium channel complex

CNGCD was previously identified as a putative interactor of CNGC15a via immunoprecipitation followed by mass spectrometry analysis using CNGC15a as a bait in *M. truncatula* roots (Charpentier lab, unpublished data). I used two approaches, bimolecular fluorescence complementation (biFC) and bidirectional yeast two-hybrid, to determine whether CNGCD is part of the calcium channel complex with CNGC15a, CNGC15b, CNGC15c and whether it can interact with DMI1.

Firstly, biFC was used to assess interaction between CNGCD and CNGC15s or DMI1 in *M. truncatula* roots. In biFC, split fluorophores fused to a protein pair of interest will reconstitute if the two proteins are in close proximity, suggesting potential direct interaction or complex formation. In earlier biFC experiments performed in *N. benthamiana* pavement cells, it was seen that CNGCD can localise in close proximity with CNGC15s and DMI1 (Charpentier lab, unpublished data). In these experiments interaction between CNGCs was only seen when half Venus was fused at the N-terminus of CNGC15s and CNGCD. Fusion of the half Venus to the C-terminus of CNGCs did not lead to Venus reconstitution, so *CNGCD:Venus^{N}/CNGCD:Venus^{C}* was used as a negative control for interaction in these experiments (Fig. 3).

To confirm earlier biFC results, the constructs previously generated were expressed in R108 *M. truncatula* roots via *A. rhizogenes* mediated transformation, and fluorescent protein reconstitution was assessed via laser scanning confocal microscopy (Figs. 2&3). Venus reconstitution was seen at the nuclear envelope in root hairs of *M. truncatula* hairy roots expressing a combination of CNGCD with CNGC15a, CNGC15b and CNGC15c, as well as with DMI1 (Fig. 2). The expression of Venus^{N}-tagged proteins was confirmed by Western blot, but Venus^{C}-tagged proteins were not detected due to nonspecific binding of the antibody used (Fig. 4). In future, another antibody to detect Venus^{C} should be used. No Venus reconstitution was observed in the roots expressing the CNGCD with half Venus fused to the C-term of CNGCD (Fig. 3).

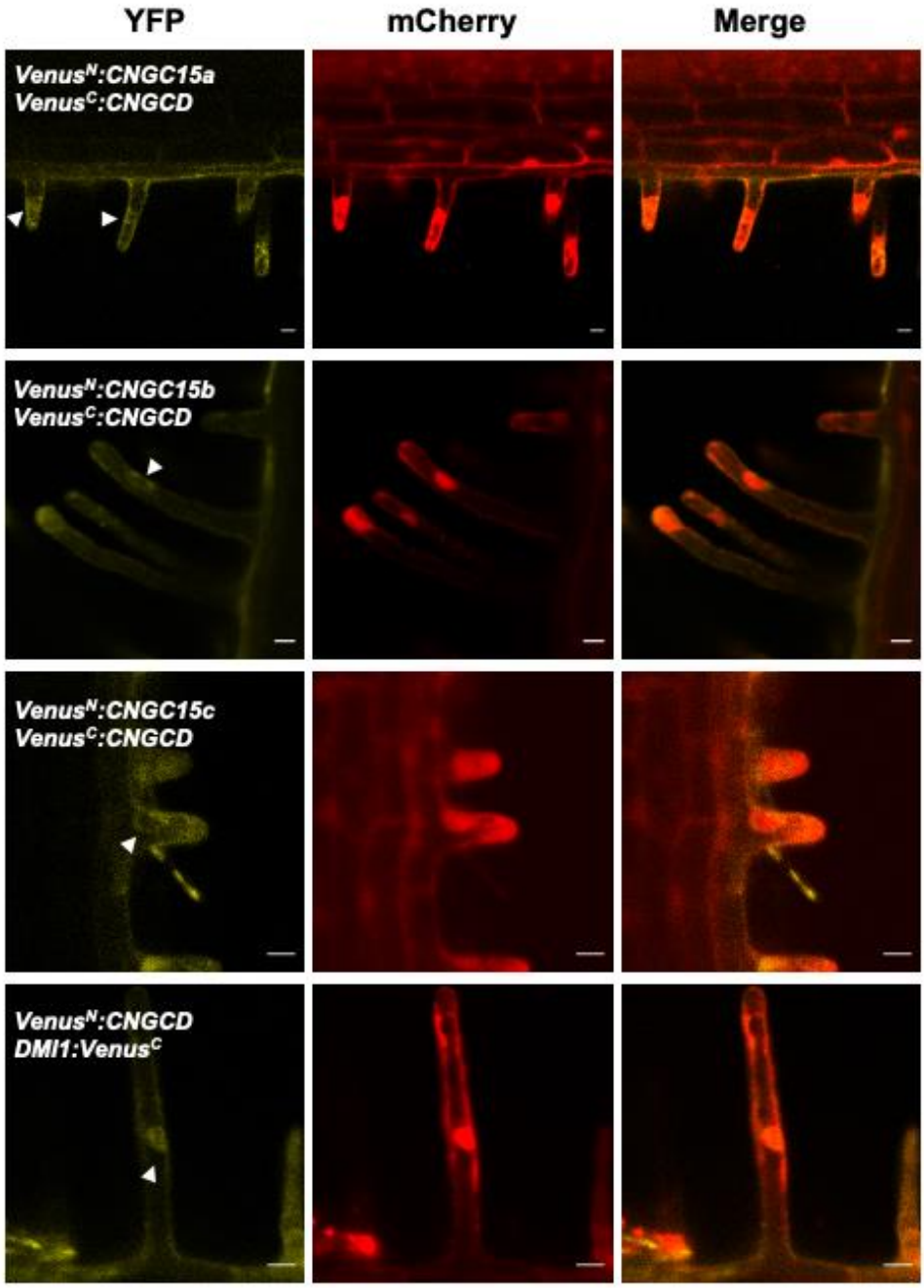


Figure 2. Pairwise interaction between CNGCD and CNGC15s and DMI1 by bimolecular fluorescence complementation. N- and C-terminal Venus ($Venus^N$ and $Venus^C$) were fused to the N-terminus of the coding sequence of each CNGC and the C-terminus of DMI1, respectively. All fusion proteins were expressed under constitutive promoters (*Lotus japonicus ubiquitin* or *Arabidopsis nopaline synthase*, see Appendix 1 for construct information). Images were taken of elongating, immature root hairs in the infection zones of *M. truncatula* hairy roots. mCherry was used as a transformation marker. The first column shows fluorescence in the yellow fluorescent protein (YFP) channel, with arrowheads indicating nuclei of root hairs. The second column shows mCherry fluorescence in the imaged root hairs, and the third column shows an overlay of the channels in the first two columns. Construct pairs are listed in the top left corner of each row. All scale bars are 10µm.

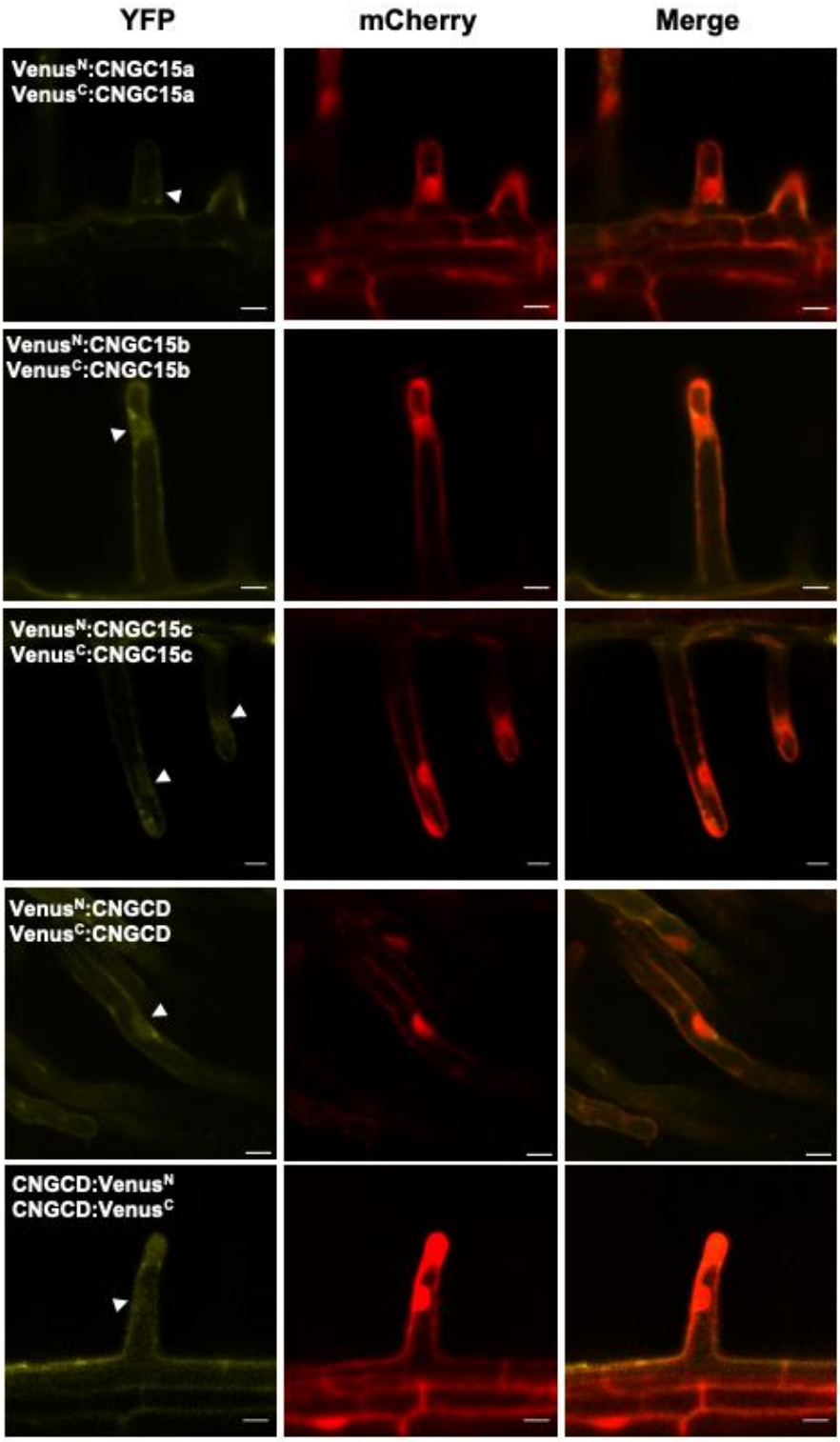


Figure 3. Self pairwise interaction of CNGC15s and CNGCD by bimolecular fluorescence complementation. N- and C-terminal Venus ($Venus^N$ and $Venus^C$ were fused to the N-terminus of the coding sequence of each CNGC and the C-terminus of CNGCD as a negative control (bottom row). All fusion proteins were expressed under constitutive promoters (*Lotus japonicus ubiquitin* or *Arabidopsis nopaline synthase*). Images were taken of elongating, immature root hairs in the infection zones of *M. truncatula* hairy roots. mCherry was used as a transformation marker. The first column shows fluorescence in the yellow fluorescent protein (YFP) channel, with arrowheads pointing at nuclei of root hairs. The second column shows mCherry fluorescence in the imaged root hairs, and the third column shows an overlay of the channels in the first two columns. Construct pairs are listed in the top left corner of each row. All scale bars are 10µm.

Interestingly, interaction was observed between CNGC15b and itself, and CNGCD and itself, but not between CNGC15a and itself, or between CNGC15c and itself (Fig. 3). This is similar to findings in earlier biFC in *N. benthamiana* (Charpentier lab, unpublished data). However, in both combinations of *Venus^{N}:CNGC15a/Venus^{C}:CNGC15a* and *Venus^{N}:CNGC15c/Venus^{C}:CNGC15c*, Western blot analysis revealed that *Venus^{N}:CNGC15a* and *Venus^{N}:CNGC15c* were either poorly expressed or absent in those samples (Fig. 4). Therefore, these pairwise interactions will require further analysis to reach any conclusion.

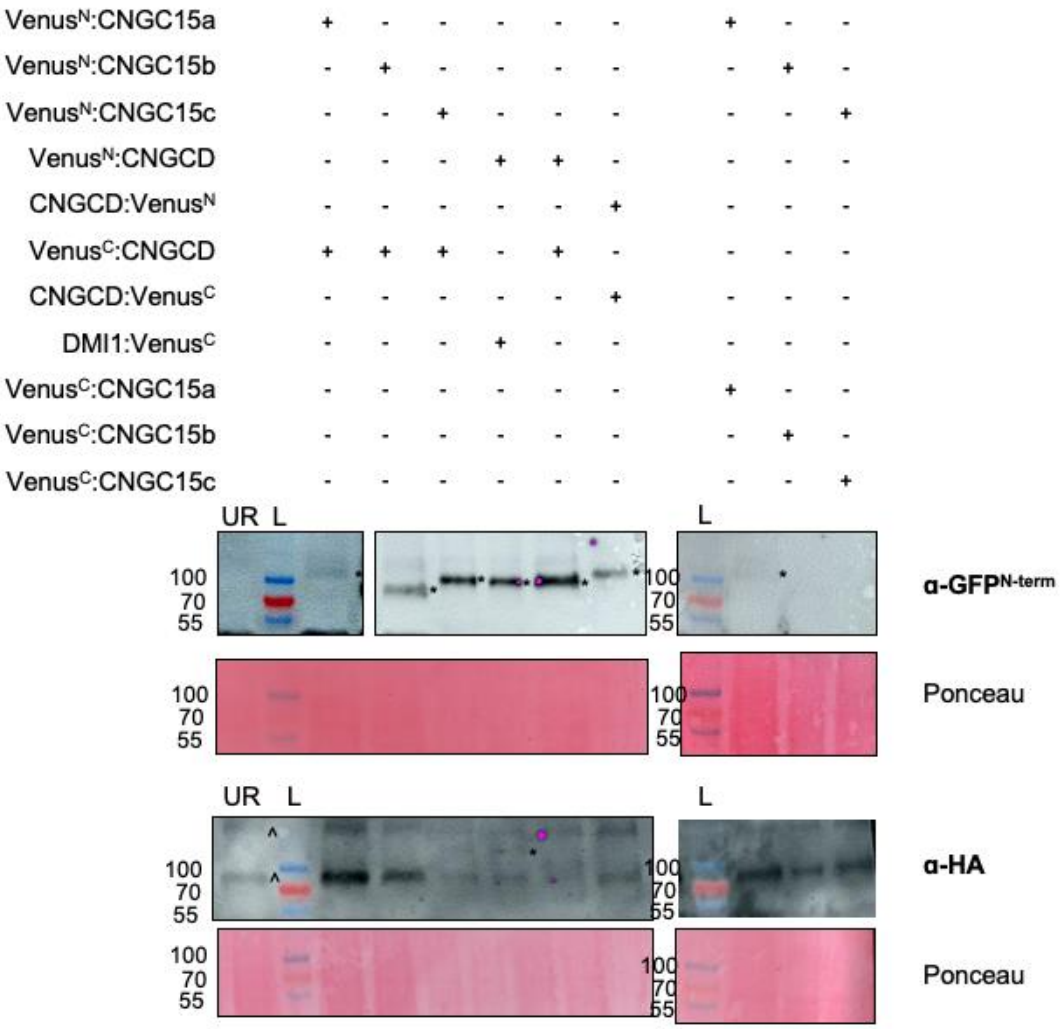


Figure 4. Western blot of bimolecular fluorescence complementation (biFC) fusion proteins (Figs 2&3). Total protein from transformed root material was extracted and separated by SDS-PAGE, transferred to nitrocellulose membranes and probed with antibodies for green fluorescent protein N-terminus (α-GFP$^{N\text{-}term}$) binding to Venus N-terminus (Venus^{N}) and haemagglutinin (HA) to bind Venus C-terminus (Venus^{C}). BiFC pairs run in each lane are indicated by +. Protein material from untransformed *M. truncatula* roots (UR) were run as a negative control. Protein ladders (L) kDa values are indicated to the side of each membrane. Positive bands are indicated by *. Unspecific bands are indicated by ^ in the control lane. Ponceau staining of membranes was used to confirm approximately equal protein loading in all wells.

Secondly, direct interaction between CNGCD and DMI1 was assessed using GAL4-based yeast two hybrid system. GAL4 is a transcription factor with two separate domains, a DNA-binding domain (BD) that binds to the promoter sequence of the target gene, and the transcription-activation domain (AD) that is responsible for the activation of transcription (Osman, 2004). These domains must function together for transcriptional activation to occur, and when fused to two proteins of interest, transcriptional activation only occurs if there is protein-protein interaction between the proteins of interest. In this experiment, when the fusion proteins interact, and BD and AD are brought into close proximity, transcription of *HIS3* and *ADE2*, histidine and adenine biosynthesis genes, is activated. These two amino acids are essential for yeast to grow, and when the transformed yeast is plated on media lacking leucine, tryptophan, adenine and histidine (-LWAH) there will only be growth if AD- or BD-fused proteins interact. Plates lacking leucine and tryptophan (-LW) are used as controls for transformation as the plasmids containing the fusion proteins of AD and BD contain either leucine or tryptophan, respectively.

The C-terminal domain (Ct) of DMI1 was subcloned into pDEST destination vector containing GAL4-AD and N-terminal domain of CNGCD (Nt) into a pDEST destination vector containing GAL4-BD. As a positive control, the SV40 large T-antigen (Clontech™ PT30234-1) and its positive interacting partner p53 were included. P53 and the T-antigen were also included in combination with CNGCD (Nt) as a negative control, to test for autoactivation. If the yeast grew in the negative control, the interaction was deemed autoactive (Fig. 5). When $CNGCD^{Nt}$ and $DMI1^{Ct}$ were co-expressed, yeast growth was observed in -LWAH, demonstrating that DMI^{Ct} can physically interact with $CNGCD^{Nt}$ to activate transcription in yeast (Fig. 5). No growth was seen when $CNGCD^{Nt}$ was expressed with either murine T-antigen or p53 (Fig. 5). These support the finding that CNGCD N-terminus interacts with DMI1 C-terminus in biFC (Fig. 2) and are similar to DMI1 interaction with CNGC15s in yeast (Charpentier et al., 2016).

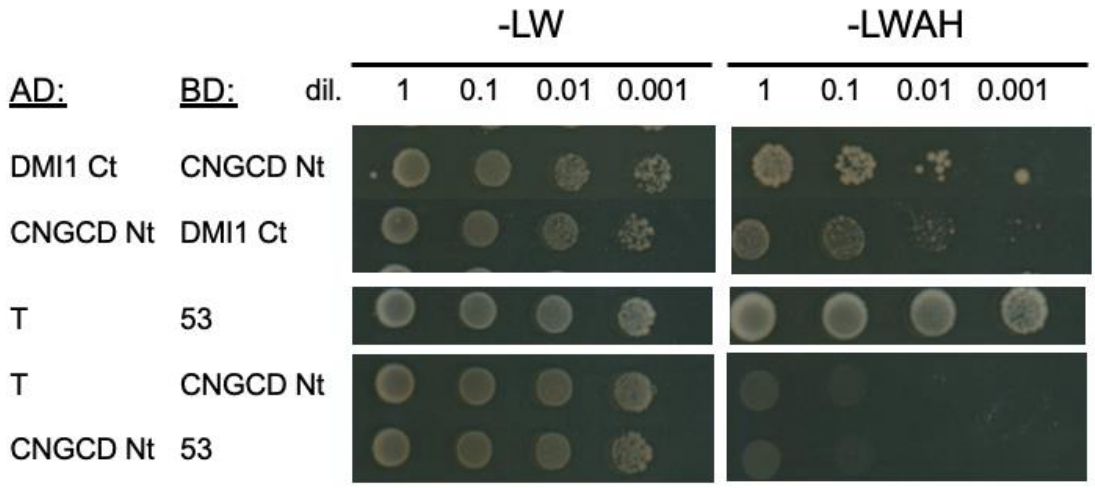


Figure 5. CNGCD N-terminus interaction with DMI1 C-terminus in pairwise GAL4-based yeast two-hybrid system. *Saccharomyces cerevisiae* strain AH109 transformed with *CNGCD N-terminus* and *DMI1 C-terminus* fused to the *Gal4 activating domain* (*AD*) and *binding domain* (*BD*) were grown on synthetic defined (SD) media deficient in leucine and tryptophan (-LW) and deficient in leucine, tryptophan, alanine and histidine (-LWAH). A ten-fold serial dilution of each resuspended pellet was plated. Murine *p53* and *SV40 large T-antigen* were used as a positive control, and *CNGCD N-terminus* and *T* or *53* were used as negative controls. The protein domain fused to the AD and BD in each row is listed to the left.

Taken together, my results suggest that CNGCD forms part of the calcium channel complex with CNGC15a, CNGC15b and CNGC15c, and interacts with the counter-ion channel DMI1.

2.3. Phenotyping of *cngcD* mutants

2.3.1. Phenotyping of *cngcD* EMS mutant lines

Next, the symbiotic phenotype of *cngcD* was assessed to understand its role in regulating RNS, AMS or both.

To assess whether CNGCD plays a role in endosymbioses signalling, a collection of *cngcD* EMS mutant lines were previously generated and backcrossed with the wild type A17 line expressing the calcium reporter Yellow Cameleon (YC) 3.6 (A17 x YC3.6). Among those backcrossed lines generated, four lines carrying missense mutations in

non-conserved amino acid residues were assessed for their nodulation phenotype at 14 dpi (Fig. 6a) and three lines for AM phenotype at 10 wpi (Fig. 6b). No significant differences in nodule number were seen among the mutant lines and the wild-type controls (One-way ANOVA, F = 1.445, p = 0.2115) (Fig. 6a), suggesting that the individual amino acid substitutions in CNGCD in these lines have no impact on nodulation at 14 dpi. No significant differences in intraradical hyphal colonisation (One-way ANOVA, F = 1.1772, p = 0.335), arbuscule colonisation (One-way ANOVA, F = 0.8578, p = 0.4973) or vesicle colonisation (One-way ANOVA, F = 1.4247, p = 0.243) at 10 wpi (Fig. 6b) were found among lines *cngcD1-3* and the wild-type controls. However, fungal colonisation among all lines was low, averaging at 25.7% for intraradical hyphae and 11.8% for arbuscules in the A17 x *YC3.6* control. Future experiments with these lines may use a more effective inoculum, to see a larger effect size where single amino-acid substitutions may cause a weak overall phenotype.

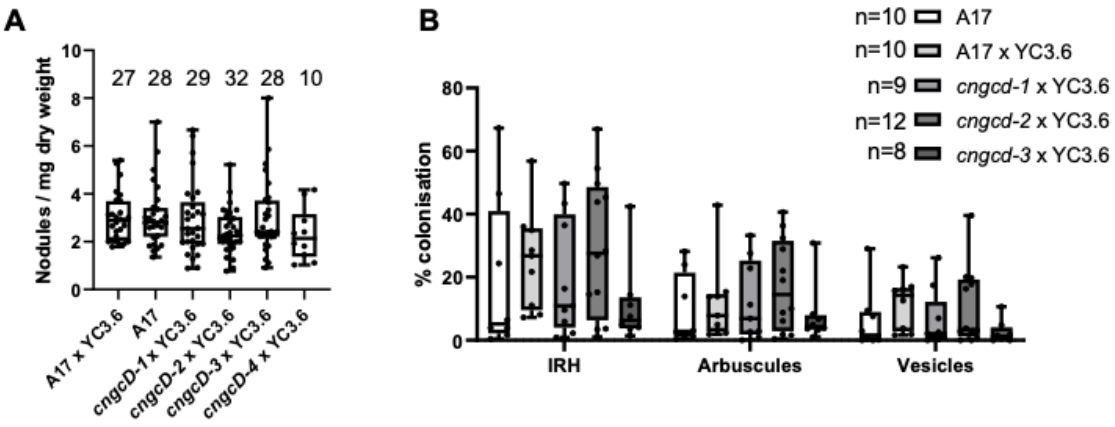
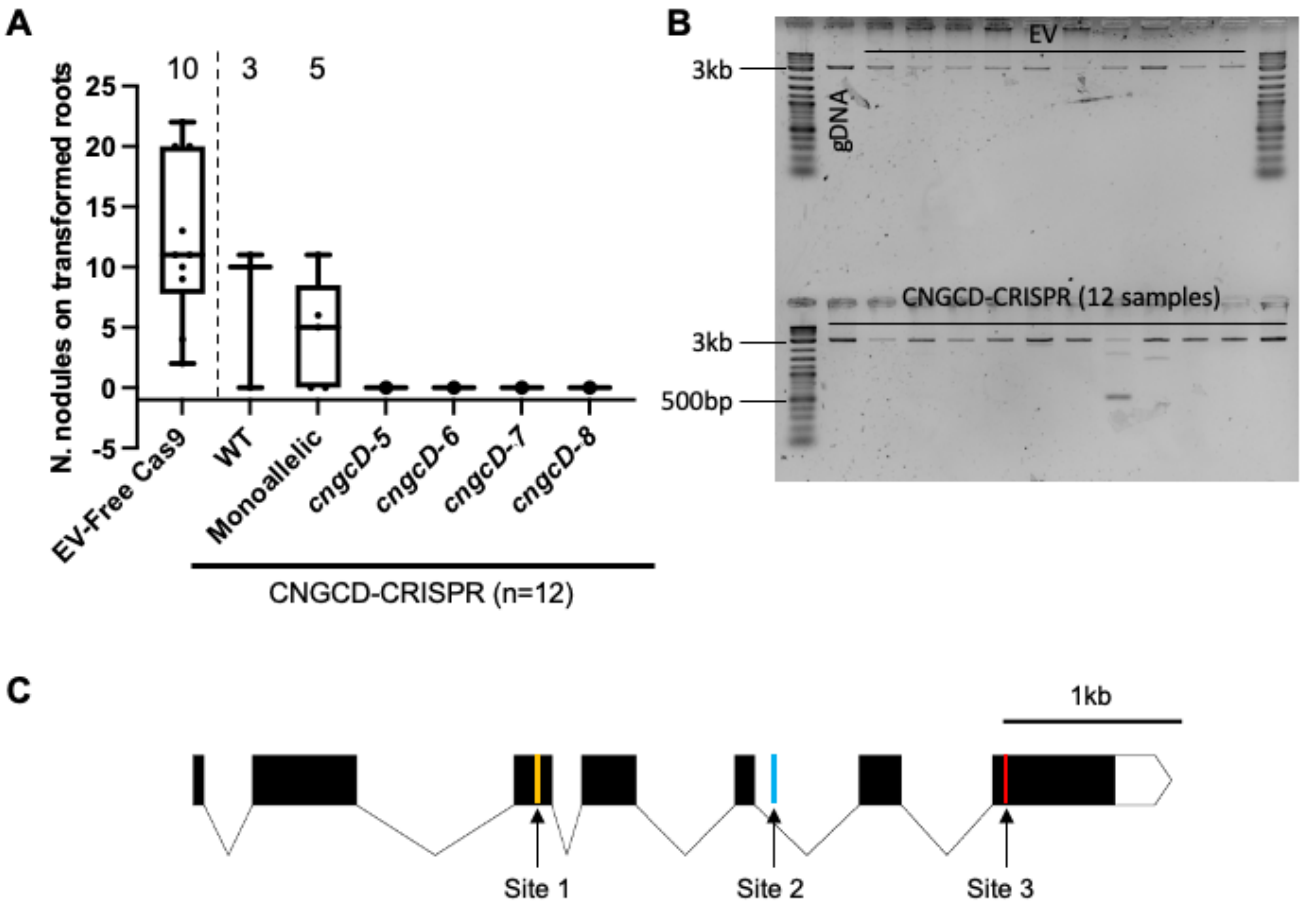


Figure 6. Nodulation (A) and mycorrhizal colonisation (B) in backcrossed EMS mutant *cngcD* x YC3.6 lines. (A) Number of nodules relative to dry weight was assessed 14 days post-inoculation (dpi) with *Sm*2011. All genotypes include data from three separate experiments, combined, except for *cngcD-4* which is only included in one replicate. Numbers of plants is shown above bars. (B) Percentage colonization of intraradical hyphae (IRH), arbuscules and vesicles in three *cngcD* x YC3.6 lines and WT A17 and A17 x YC3.6 at 10 weeks post-inoculation with *Rhizophagus irregularis*. n = number of roots assessed. Means were compared using one-way ANOVA followed by Dunnett's post-hoc test with A17 x YC3.6 used as the control variable. Non-significant pairwise comparisons not shown.

2.3.2. CRISPR-Cas9 of *cngcD* in hairy roots

Given the unlikelihood of identifying a mutant phenotype from a single substitution induced by EMS, CRISPR/Cas9 was used as a strategy to generate knock-out *cngcD* and assess the nodulation phenotype. Cas9 can cause small insertions or deletions at sites of double-strand breaks (DSBs), causing a frameshift (Doudna and Charpentier, 2014). *M. truncatula* R108 roots were transformed with a CRISPR/Cas9 construct previously generated, containing three sgRNAs and Cas9 (*CNGCD-CRISPR*), and an empty vector, containing Cas9 with no sgRNAs (*EV-Free Cas9*). Nodulation was assessed in transformed roots 28 dpi, and transformed roots genotyped to confirm if Cas9 had caused misrepair of DSBs at sgRNA sites (Fig. 7). There are no significant differences between nodule numbers on EV-transformed roots, and wild-type and monoallelic roots transformed with *CNGCD-CRISPR* (Kruskal-Wallis; $H = 4.359$, $p = 0.113$). However, the number of roots included may be too low to indicate whether heterozygous *cngcD* mutation has an impact on nodulation, and this should be investigated further using segregating populations of *cngcD* stable mutants.



D

		Site 1	Site 2	Site 3	
cngcD-5	allele 1	+1		-3	Frameshift, early termination
	allele 2			-2	Frameshift, early termination
cngcD-6	allele 1	-6			In-frame deletion of 2 residues
	allele 2	+1			Frameshift, early termination
cngcD-7	allele 1			-3	In-frame deletion of 1 residue
	allele 2	--	--	--	Excision of 1.3kb
cngcD-8	allele 1	+1			Frameshift, early termination
	allele 2			-3	In-frame deletion of 1 residue

Figure 7. Nodulation in hairy roots expressing *Cas9* and gRNAs targeting *CNGCD*. (A) Number of nodules on roots transformed with *Cas9* (EV-Free Cas9) or *Cas9* and gRNAs targeting CNGCD (CNGCD-CRISPR) and inoculated with *Sm*2011 for 28 days. Means of *EV-Cas9*, WT and monoallelic *CNGCD-CRISPR* were compared using Kruskal-Wallis test with post-hoc comparisons. (B) PCR of a 3.1kb fragment of *CNGCD* from EV control roots (top row) and roots transformed with *CNGCD-CRISPR* (bottom row). PCR of gDNA is included as an additional control. (C) Location of gRNAs on CNGCD. (D) Description of insertions and deletions at each gRNA site in *cngcD* biallelic mutant roots, on which no nodules formed.

9/12 root systems well transformed with the CNGCD-CRISPR construct had monoallelic or biallelic insertions or deletions, giving an efficiency of 75% (Fig. 7a). I found four individual root systems, from 12 plants transformed with the CNGCD-CRISPR construct, that had biallelic insertions or deletions at sgRNA sites, named *cngcD-5—8*. All had no nodules on transformed roots (Fig. 7a). This indicates that homozygous *cngcD* knockout may create a nodulation-deficient mutant, and suggests a function for CNGCD in nodulation. However, some monoallelic and wild-type roots transformed with this construct also had no nodules on transformed roots, likely due to poor growth of the transformed root system in these individuals (Fig. 7a). Future work assessing nodulation in *CNGCD-CRISPR* hairy roots should use a larger number of transformed roots and ensure that all inoculated plants have the opportunity to grow nodules. This is to confirm that a loss of nodulation is due to knockout of *cngcD* and not poor growth of the transformed roots.

PCR genotyping of transformed roots showed large deletions in some roots containing the *CNGCD-CRISPR* construct (Fig. 7b). Sanger sequencing was used to determine whether roots transformed with the *CNGCD-CRISPR* construct had wild-type sequence at the three sgRNA sites, or if there were mono- or bi-allelic mutations (Fig. 7c, d). Sanger sequencing of *cngcD-5—8* identified some alleles with frameshifts leading to early termination and likely non-functional proteins (Fig. 7d). Three roots had monoallelic deletions that were visible by gel electrophoresis (Fig. 7b). One monoallelic root showed excision of the entire 2.6kb region between sgRNA 1&3, and *cngcD-7* showed a 1.3kb deletion on one allele (Fig. 7d). However, some repairs of DSBs led to in-frame deletions of one or two residues, so it is unclear if these led to non-functional proteins (Fig. 7d). I found no evidence of insertions or deletions at site 2, suggesting that this sgRNA may be ineffective at targeting Cas9 to *CNGCD* (Fig. 7d).

Taken together, these suggest that homozygous *cngcD* may be nodulation-deficient, but to increase confidence in these results, a stable mutant knockout line should be assessed.

2.3.2. Generation of *cngcD*-CRISPRCas9 stable lines

A new construct was made, with sgRNAs targeting sites 1 and 3, given that these were found to be effective in causing DSBs in my and earlier experiments (Charpentier lab, unpublished data). The construct was stably transformed by *A. tumefacians*-mediated transformation (transformation performed by Nicola Cook, Charpentier group).

I genotyped the T_0 generation by amplifying *Cas9* and a fragment of *CNGCD* containing both sgRNA sites by PCR. If a plant had *Cas9* inserted, I sequenced *CNGCD* around sgRNA sites to find evidence of small insertions or deletions. 30 T_0 plants were produced from the original transformation, of which 25 were genotyped and 5 died before genotyping. 25/25 T_0 plants had *Cas9* inserted and detectable by PCR, and 0/25 had visible insertions or deletions when sgRNA sites were sequenced.

Since I did not identify a monoallelic or biallelic *cngcD* mutant among the T_0 generation, and *Cas9* is inserted in all the lines tested, I produced T_1 populations from the transformed plants. Cas9 and the sgRNAs may be expressed in the germline and able to cause mutations in the T_1 generation, additionally, chimeras are likely in the T_0 generation (Čermák et al., 2017; Feng et al., 2018). I then generated T_1 populations from four T_0 parents, selected for their high expression of the RUBY transformation marker, which may thus indicate higher expression of Cas9. I observed segregation of the purple RUBY colour phenotype in the T_1 generation. Although 120/124 T_1 plants had *Cas9* inserted in their genome, I did not identify a *cngcD* mutant among the 120 plants which were all sequenced (Table 1). I created T_1 populations from 10 additional T_0 parents but was not able to genotype these plants in the time allowed. Future work may thus identify a *cngcD* mutant among T_1 populations not yet genotyped.

Table 1. Summary of genotyping of T_1 plants transformed with CRISPR constructs targeting *CNGCD*.

Parent	**Cas9 detectable by PCR / total plants**	**Indels detected by Sanger sequencing / total sequenced**
1	25/26	0/25
2	34/35	0/34
3	24/25	0/24
4	37/38	0/37

3. Discussion

Here I have begun to characterise CNGCD and its role in root endosymbioses in *M. truncatula*. Taken together, my results suggest a role for CNGCD in root endosymbioses. The *CNGCD* promoter is active in symbiotic tissues (Fig. 1), and CNGCD interacts with components of the nuclear calcium signalling machinery *in planta* (Fig. 2) and in yeast (Fig. 5). Knockout of *cngcD* in hairy roots leads to loss of nodulation, suggesting a function in root nodule symbiosis (Fig. 7). However, much work is needed to understand the stoichiometry of the calcium channel in symbiosis signalling, and what role, if any, CNGCD plays in generating nuclear calcium signals.

The expression pattern of *CNGCD* in nodules differs to that of *CNGC15a, b* and *c*. My observation of *CNGC15a, b* and *c* expression concentrated in the nodule meristem (Fig. 1a) concurs with previous experiments expressing these *promoter:GUS* constructs in nodule tissues. I found *CNGCD* expression to be expressed more diffuse through the nodule (Fig. 1a). In support of this finding, *CNGCD* is significantly expressed in all nodule regions, without significantly high expression in any nodule region in comparison with another, in laser-capture coupled RNA-seq data by Roux et al. (2014). I also observed that staining of nodules took much less time for *pCNGCD:GUS* nodules than *pCNGC15:GUS* nodules, suggesting that *CNGCD* may have higher expression in nodules than the *CNGC15*s. Concurrent with this, *CNGCD* shows higher expression in nodules in RT-qPCR experiments (data not shown) and across experiments in the Medicago Gene Expression Atlas (Carrere et al., 2021). Recent advances in single-cell transcriptomics can give further insight into the expression patterns of *CNGCs* in different tissue layers and stages of infection. A recent single-nucleus RNA-sequencing study identified *CNGC15c* as highly enriched in the epidermis independent of rhizobial inoculation, suggesting that *CNGC15c* is enriched in the epidermal layer prior to infection with rhizobia (Cervantes-Pérez et al., 2022). *CNGCD* is also upregulated in a cortical cell cluster in response to rhizobia (Cervantes-Pérez et al., 2022). Such datasets will be useful for forming hypotheses about the role of each component in the epidermis and cortex in future experiments, and as a point of comparison when interpreting results. The expression pattern of *CNGCD* compared with *CNGC15s* may also be further assessed by confocal microscopy using GFP-protein fusions under the control of native promoters.

I describe CNGCD interaction with CNGC15a, b and c and DMI1 in *in planta* biFC experiments (Fig. 2). Venus reconstitution in *N. benthamiana* leaves only occurred when fluorophores were fused to the N-terminus of CNGCs in earlier experiments (Charpentier lab, unpublished data). Similarly, in my experiments, Venus reconstituted when fused to the N-terminus, and not when fused at the C-terminus of CNGCD (Figs. 3,4). This suggests that the N-terminal domains of these CNGCs are in close proximity in a heterotetrameric complex, and that the C-terminal domains are too far apart to allow Venus reconstitution. To confirm if N-terminal domains physically interact, future experiments may examine the effect of deleting the N-terminus on interaction in *in planta* co-immunoprecipitation (coIP).

Little is known about inter-subunit interaction and required domains for tetramerisation in plant CNGC tetramers due to a lack of structural information, though some studies have started to answer this question. Plasma membrane-localised CNGC8-CNGC18 heterotetramer subunits interact via their C-termini in *Arabidopsis* and C-terminal regions appear to be required for heterotetramer formation (Pan et al., 2019). N-termini of LjBRUSH, a *L. japonicus* CNGC, interact in yeast two-hybrid assays (Chiasson et al., 2017).

In related channels in animals and prokaryotes, inter-subunit interaction typically occurs between domains in the C-terminus. In animal rod and cone CNG channels, three CNGA1 and one CNGB1, or three CNGA3 and one CNGB3, units form the rod and cone channels respectively (Weitz et al., 2002; Ding et al., 2012). A C-terminal leucine zipper (CLZ) domain in the CNGA1/CNGA3 subunits determine the 3:1 stoichiometry by creating a 3-helix coiled coil (Zhong et al., 2002; Shuart et al., 2011; Xue et al., 2022). When the CLZ is removed, alternate stoichiometries can form (Shuart et al., 2011). In the *C. elegans* TAX-4 channel, interaction occurs between transmembrane domains and between gating rings in the C-linker region of each subunit (Li et al., 2017). In the human HCN1 homotetramer, linkers between two transmembrane domains of one subunit interact with C-linker and CNBD from an adjacent subunit (Lee and MacKinnon, 2017). In contrast, the CNBDs in prokaryotic cyclic-nucleotide gated channel LliK are rotated outward and facing away from each other, preventing interdomain interaction, while there remains intersubunit interaction between C-linkers (James et al., 2017). In contrast, my biFC data suggest that C-terminal domains are not in close enough proximity to physically interact (Figs. 2&3).

More detailed structural data from cryo-EM or x-ray crystallography in future will determine how CNGC15 and CNGCD subunits interact and what structural features determine stoichiometry.

CNGCD interaction with CNGC15a, b and c *in planta* suggests that CNGCD forms a heterotetramer with CNGC15a, b, c in a specific, as yet unknown, stoichiometry. Heterocomplexes in calcium channels might allow specific calcium signatures, from each subunit being differently regulated through protein-protein interaction and forming a channel with unique ion conductance and gating. Specific heterotetramers might form sensing complexes with receptor kinases and other membrane proteins, creating a membrane nanodomain that senses a specific elicitor and generates a specific calcium signal. Aberrant calcium spiking in root hairs of *cngc15* single mutants suggests that all three subunits make up part of the epidermal nuclear calcium channel in Nod factor sensing (Charpentier et al., 2016). Given that calcium spiking in root symbioses shows different signatures in the epidermis and cortex during progression of the symbiont, it is possible that multiple channels with unique stoichiometries control the calcium signatures in each cell layer (Sieberer et al., 2012). My expression analysis using *pCNGCD:GUS* did not focus on native *CNGCD* expression in the root prior to symbiont infection, so does not reveal whether *CNGCD* is natively expressed in epidermal or cortical cell layers (Fig. 1). GFP-fused *CNGCD* under its native promoter should be analysed by confocal microscopy in future experiments to establish whether *CNGCD* is expressed in the epidermis or cortex and therefore where it interacts with CNGC15s.

CNGC heterotetramers have been implicated in several processes in *Arabidopsis*, including CNGC2/4/6 in immunity and thermosensing, CNGC2/4 in floral growth, CNGC18/7/8 in regulation of pollen tube growth, CNGC6/9/14 in root hair growth, CNGC5/6/9/12 in ABA-induced stomatal closure (Chin et al., 2013; Brost et al., 2019; Pan et al., 2019; Tian et al., 2019; Ma et al., 2023; Tan et al., 2023). Despite this, few reports can conclude the stoichiometry of any one calcium channel, given that individual subunits may form functional homotetramers when expressed in *X. laevis* oocytes, or they may bind promiscuously with several other CNGCs. CNGCs can be implicated in multiple biological processes or expressed in many tissues, meaning they might form heterotetrameric channels in some contexts and not others. CNGCs that do not form a heterotetramer in any known context might retain the ability to bind to one

another—when constitutively expressed *in planta* or when co-expressed in a heterologous system such as yeast—from the evolutionary expansion of CNGCs in plants, rather than a biological function. In future it will be important to combine cell layer-specific expression data with protein-protein interaction assays using CNGC15s and CNGCD under the control of their native promoters.

My biFC data suggest that there are limitations on self-interaction, which may imply limits on complex formation *in planta* (Fig. 3). While CNGCD and CNGC15b can interact with themselves in biFC experiments, CNGC15a and CNGC15c do not. Additional *in planta* coIP should confirm whether there are physical limitations on pairwise interactions between CNGC15s and CNGCD. Given that expression of $Venus^{N}$:CNGC15a and $Venus^{N}$:CNGC15c could not be confirmed by Western blot (Fig. 4), due to small tissue sample used, it cannot be ruled out that this negative result is due to incorrect expression of the protein construct. Additionally, none of the $Venus^{C}$ fusion constructs, apart from DMI1:$Venus^{C}$, could be detected by Western blot (Fig. 4) due to non-specific binding of the antibody, so it is possible that negative results were due to incorrect or insufficient expression of $Venus^{C}$ fusion constructs. CNGC15a can form a calcium-permeable homotetrameric channel in *X. laevis* oocytes, in contrast with biFC results in both *M. truncatula* and *N. benthamiana* (Charpentier et al., 2016). This either suggests a limitation with the *in planta* biFC system, such as Venus inhibiting interaction between subunits or tetramerisation at the C-terminus, or highlights the importance of studying protein-protein interaction *in planta*, where native post-translational modification may limit interaction between proteins that can interact in a heterologous system.

A limitation of these experiments is the use of constitutive promoters for biFC constructs, since a large quantity of fluorophores must reconstitute to be visible in confocal microscopy and native expression of each ion channel is low. This means it is not possible to confirm the cell layer that interaction is happening, since protein pairs are being ubiquitously expressed in all cells, and does not confirm if these proteins interact under their native promoters. Furthermore, individual CNGC subunits may be implicated in multiple biological processes and some CNGCs can bind other CNGCs promiscuously (Tan et al., 2023). Future work might aim to dissect where the CNGCs of interest in this study, CNGC15s and CNGCD, are natively interacting with each other, in particular, in the epidermis or cortex, in root nodule symbiosis or AM

symbiosis, or in early or late stages of symbiotic infection. One way to achieve this is to assess pairwise interaction using coIP with CNGCs under the control of their native promoters. An alternative approach might use TurboID fused to CNGCs under control of epidermis-specific and cortex-specific promoters to label native interacting proteins in each cell layer (Mair et al., 2019).

Furthermore, reconstitution of Venus may be possible over larger distances than would suggest physical interaction, especially with a flexible linker (Kerppola, 2006). BiFC is still preferable to Förster resonance energy transfer (FRET)-based microscopy techniques while there is limited structural knowledge about where CNGC subunits interact. FRET is only detectable over distances of ~100Å and therefore a more accurate microscopy technique for studying protein-protein interaction (Kerppola, 2006). As structural knowledge of plant CNGCs improves, future work might use FRET to study the physical interaction between CNGC subunits and the impacts of deletion of putative domains required for tetramer formation.

Yeast two-hybrid data suggest that CNGCD and DMI1 interact via CNGCD N-terminus and DMI1 C-terminus (Fig. 5), consistent with DMI1 C-terminus interaction with CNGC15s N-termini (Charpentier et al., 2016). I did not see pairwise interaction between CNGC N-termini in yeast in my own experiments (data not shown), possibly due to poor expression or instability of the protein fusion in yeast. In contrast, the N-terminus of LjBRUSH can interact with itself in yeast two-hybrid assays (Chiasson et al., 2017).

My results suggest that *cngcD* might be nodulation-deficient in hairy roots (Fig. 7a). In comparison, single mutants in *cngc15a, b* and *c* are not completely deficient in nodulation, AM colonisation, or rhizobial infection, and show abnormal calcium spiking (Charpentier et al., 2016). If my finding is replicated in future experiments using a stable mutant line, this might mean that CNGCD is an essential component for the calcium channel in nodulation, whereas CNGC15a, b and c have partially redundant functions in root endosymbioses. Similarly, in other processes where CNGC heterotetramers are implicated, mutants in individual components show differing levels of redundancy. For example, CNGC7/8 are redundant in regulating pollen tube growth while a single mutant of *cngc18* is male sterile, and CNGC6/9/14 are partially redundant in root hair growth (Brost et al., 2019; Pan et al., 2019). My data are consistent with a hypothesis that each component of a heterotetrameric channel is

required for correct calcium signalling. Loss of individual CNGC15s may create an abnormally functioning channel, while loss of CNGCD might prevent tetramerisation or sensing. Future work should examine *cngcD* phenotype in AM colonisation, rhizobial infection and calcium spiking in response to Nod factor, in addition to crosses with *cngc15* single and double mutants, to further understand the requirement for CNGCD in calcium signal generation in symbioses. Future work might also assess the impact of putative interaction domains in CNGCD, required for tetramerisation or sensing, to determine which protein-protein interactions are essential for the generation of calcium signals.

Results of targeting *CNGCD* using CRISPR/Cas9 in hairy roots, both in my experiments and in others, suggest that sgRNAs 1&3 are effective in creating DSBs in the sequence of *CNGCD* and can therefore be used to make a stable *cngcD* mutant (Fig. 7d). I saw high efficiency of Cas9 in hairy roots, with 75% of plants effectively transformed with CNGCD-CRISPR showing indels on one or both alleles (Fig. 7a). However, I was not able to identify a mutant among the T_0 or T_1 plants genotyped (Table 1). Most reports using CRISPR/Cas9 to knock out genes in *M. truncatula* use the hairy root system, which creates mutant root systems with high efficiency (Jardinaud et al., 2022; Pecrix et al., 2022). Several reports also describe successful generation of stable single- and multi-gene knockouts with high efficiency (Meng et al., 2017; Zhu et al., 2021). Without a comparison of efficiency of a CRISPR/Cas9 knockout of the same target using *A. rhizogenes*- vs *A. tumefaciens*-mediated transformation it is not possible to say whether the efficiency of mutation is higher using one transformation method over the other. In future experiments, more attention could be paid to the RNA expression of Cas9, as a proxy for protein expression, when selecting T_0 parents without detected mutations. Several reports suggest higher efficiency of CRISPR/Cas9 in the T_1 generation, particularly in cereals, suggesting that a *cngcD* mutant might be found among the T_1 populations not yet genotyped (Feng et al., 2018). Additionally, many genotype only in the T_1 generation due to the likelihood of chimeras in the T_0 (Čermák et al., 2017).

4. Materials and Methods

Plant material and growth conditions

M. truncatula R108 seeds were scarified using sandpaper and surface-sterilised in 10% sodium hypochlorite + 0.1% Tween-20 for 10 minutes and rinsed 6x with sterile deionised H_2O. Seeds were imbibed for 6-8 hours in 5 μg/mL nystatin + 50 μg/mL augmentin and rinsed 3x with sterile deionised H_2O. The seeds were then spread evenly onto water agar plates containing 3% agar, 5 μg/mL nystatin + 50 μg/mL augmentin, the plate inverted and covered. After 4 days of stratification in the dark at 4°C, seeds were germinated at room temperature in the dark, with the plate still inverted.

Germinated seeds were transferred to Modified Fahraeus Medium (FP) media + 5 μg/mL nystatin (without nystatin if plants were later inoculated with AM fungi) and were grown at 22°C, 80% humidity, 16 h photoperiod, 300 μmol m^{-2} s^{-1} light intensity.

Medicago truncatula hairy root transformation

A. rhizogenes strain AR1193 was transformed with the construct of interest by electroporation (1.25 V, resistance 200 Ω, time constant 4.8 s) and grown on lysogeny broth (LB) agar containing selective antibiotics for 3 days at 28°C. A single colony was used to inoculate liquid LB containing selective antibiotics, which was grown for 24 hours at 28°C. The liquid culture was centrifuged at 4000 rpm for 5 mins and the pellet resuspended in 1 mL sterile deionised H_2O.

The seed coat was removed from the germinated seed and the tip of the radicle cut to remove the root meristem, and the cut radicle was dipped in the *A. rhizogenes* culture for at least one minute. Seedlings were placed on plates containing Modified FP media + 5 μg/mL nystatin and grown at 22°C, 80% humidity, 16h photoperiod, 300 μmol m^{-2} s^{-1} light intensity for one week.

After one week, emerging untransformed roots were cut from the seedlings and the seedlings placed onto modified FP plates (+ 5 ug/mL nystatin unless used for AM assays) covered with filter paper to prevent the transformed roots from growing into the agar. Two weeks after transfer, the emerging roots were screened for mCherry/DsRed fluorescence using a stereo microscope.

Nodulation and arbuscular mycorrhizal colonisation assays

WT A17, A17 x YC3.6 and *cngcD* EMS lines were grown on Modified FP agar for one week before inoculation.

Well-transformed roots, positive for mCherry or DsRed expression in all root tissue layers, assessed under a stereo microscope, and at least 2 cm long and with lateral roots emerging were considered ready for transfer to trays, typically 3-4 weeks after transformation.

For nodulation assays, plants were transferred to trays (each well 45x45x50mm, with 40 cells in each tray) containing 1:1 sand:terragreen (Oil-Dri Company, Wisbech, UK). *S. meliloti* strain *Sm*2011 was grown in tryptone and yeast (TY) media containing 4 μg/mL tetracycline + 100 μg/mL spectinomycin for 3 days at 28°C, centrifuged at 4000rpm for five minutes and resuspended in deionised H_2O. 5 mL of *Sm*2011 OD_{600} = 0.01 was used to inoculate each plant. Uninoculated controls were kept in separate trays. Roots were dug out of trays at the time points indicated, rinsed and stored in water prior to counting, or immediately stained as indicated.

Nodules were counted under a stereo microscope, using brightfield (for stable lines) or DsRed fluorescence (for transformed roots – to exclude nodules on untransformed roots that emerge after planting in trays). Roots from WT and *cngcD* stable lines were dried completely at 37°C and the dry weight measured, with number of nodules expressed relative to mg dry weight. Transformed roots were flash-frozen for genotyping (*cngcD*-CRISPR in hairy roots) or qRT-PCR (for NIMIN overexpression nodulation analysis) so total nodules per transformed root system is shown instead.

Mycorrhizal colonisation was assessed 10 weeks post-incoulation (wpi) using the grid-intersect method (Giovannetti and Mosse, 1980). Roots were cleared in 10% KOH for 15 min at 95°C, rinsed 3x in water and stained in 5% acetic acid 3% ink for 10 min at 95°C, then rinsed again and stored in water before scoring. Each root system was spread out evenly over a grid and the presence of intraradical hyphae, arbuscules and vesicles was scored at each intersect, and expressed as a percentage of total intersects interrupted by a root.

Histochemical staining

Roots expressing *pCNGC:GUS* constructs were dug out of trays at 28 dpi (nodulation) and 8 wpi (AM colonisation). Roots were fixed in 90% methanol for 1 hr at -20°C and rinsed in phosphate buffer (0.5M Na_2HPO_4, 0.5 M NaH_2PO_4, 0.1M $K_3Fe(CN)_6$, 0.1M $K_4Fe(CN)_6$) for 3x10 min with gentle agitation. Roots were then stained with X-Glc (2mM 5-bromo-4-chloro-3-indolyl-beta-D-glucuronide, 0.5M Na_2HPO_4, 0.5 M NaH_2PO_4, 0.1M $K_3Fe(CN)_6$, 0.1M $K_4Fe(CN)_6$), by vacuum infiltrating for 30 min at room temperature, followed by 24 hr incubation at 37°C.

To stain fungal structures in AM-inoculated roots, after GUS staining, roots were placed in 50% ethanol overnight, then cleared in 20% potassium hydroxide for two days at room temperature. Roots were then rinsed with diH_2O, placed in 0.1M hydrochloric acid for 3 hours, rinsed again with diH_2O and 1x phosphate-buffered saline (PBS). Roots were then placed in 1x PBS containing 0.5 µg/mL WGA Alexa Fluor-488 overnight at room temperature.

GUS- and WGA- stained roots were imaged using a Leica DM6000 microscope, using a 10x air lens.

Confocal microscopy

Well-transformed roots expressing biFC constructs were imaged when ~2cm long and before lateral roots began emerging. Immature, emerging root hairs, close to the meristem, were imaged. Root hairs were imaged using a Zeiss LSM880 microscope at 40x magnification using a water immersion lens. YFP was excited using an argon laser (514 nm; laser power 30%) and emission was collected at 516-543 nm; mCherry was excited using a solid state laser (594 nm; laser power 8%) and emission collected at 600-750 nm. The pinhole was opened to 6.1 µm. Pixel dwell time on scanning was 4.10 µsec, and line-averaging from 16 scans was used to reduce noise in the final scan. Images were taken at 510x510 pixel resolution. Where brightness and contrast are adjusted post-acquisition, this was done on ImageJ and applied equally to the entire image.

Western blot

Frozen root samples were ground using a cooled mortar and pestle, then dissolved in pre-warmed extraction buffer (100 mM Tris, 150 mM NaCl, 5 mM EDTA, 10 mM DTT, 5% SDS, 4M urea, protease inhibitor) and heated at 70°C for 30 min, followed by centrifugation at 13000 rpm for 2 min. 20µL of the supernatant was mixed with 5µL sample buffer (Bio-Rad, Berkeley, USA) and heated at 90°C for 5 minutes prior to gel loading.

SDS-PAGE was run on pre-cast gels (Mini-PROTEAN TGX; Bio-Rad, Berkeley, USA) in running buffer (25 mM Tris, 192 mM glycine, 0.1% SDS, pH 8.3) for 30 min at 75V followed by 45-60 min at 130V. Transfer to nitrocellulose membrane (Bio-Rad, Berkeley, USA) was performed for 16 hours at 30V at 4°C in transfer buffer (25 mM Tris, 192 mM glycine, 0.1% SDS, 20% EtOH). The membrane was washed in Tris-buffered saline (TBS-T; 20 mM Tris, 150 mM NaCl, 0.5% Tween-20, pH 7.6) for 3x 15 min followed by a 1 hr block in TBS-T + 5% milk. The membrane was then rinsed in TBS-T for 3x5 min and incubated in the primary antibody in TBS-T + 1% milk overnight at 4°C. The primary antibody for probing the N-terminal of Venus was anti-GFP N-terminal (Rabbit, G-1544, Sigma-Aldrich, St Louis, MI, USA) at a titration of 1:1000 and the primary antibody for probing the C-terminal of Venus was anti-HA-HRP (Rabbit monoclonal, Ref:12013819001, Roche, Basel, Switzerland) at a titration of 1:500. Membranes were washed in TBS for 3x15 min. For C-term-Venus-tagged proteins membranes were incubated for 1 hr in anti-Rabbit (Mouse IgG-HRP, sc-2357, Lot A0120, Santa Cruz Biotechnology, Santa Cruz, USA) in TBS + 1% milk. For detection, membranes were covered in 2mL of SuperSignal chemiluminescence detection reagent (Thermo Fisher, Waltham, USA; 1 mL each of luminol and peroxide solution) in the dark for 5 min. Membranes were imaged on an ImageQuant LAS 500, with 45 min exposure for membranes treated with anti-GFP Nterm and 6 min exposure for membranes treated with anti-HA.

Yeast two-hybrid assay

The C-terminal domain of DMI1 (S343 to E882) and the N-terminal domain of CNGCD (M1 to F106) were previously fused to both the AD and BD of Gal4 by Gateway cloning. The SV40 large T-antigen and its positive interacting partner p53

(Clontech™ PT30234-1) were used as a positive control, and CNGCD N-terminus interaction with T and 53 used as a negative control. *S. cerevisiae* strain AH109 was grown on YPAD agar for 3 days at 28°C and a single colony was used to inoculate a liquid YPAD culture overnight at 28°C. Yeast were transformed with protein pair constructs using the lithium acetate method (Gietz and Woods, 2001) and grown on synthetic dropout (SD) agar lacking leucine (L) and tryptophan (W) for 3 days.

A single yeast colony was used to inoculate liquid double dropout (SD -LW) media overnight at 28°C. 800µL of liquid culture was centrifuged at 1000 *g* and the pellet resuspended in 500 µL sterile diH_2O. A ten-fold serial dilution was plated on double (SD -LW) and quadruple (SD minus leucine (L), tryptophan (W), alanine (A) and histidine (H)) dropout agar plates and incubated at 28°C. After 3 days growth was assessed and imaged.

Each transformation was repeated three times with similar results. Representative images are shown in Fig. 5.

Genotyping *CNGCD-CRISPR* lines

DNA was extracted from T0 and T1 plants transformed with Cas9 and guide RNAs targeting *CNGCD* using DNeasy plant mini and 96-well kits (Qiagen, Hilden, Germany). DNA samples were eluted in 30 µL deionised H_2O. PCR was used to amplify a 3.1kb region containing all 3 gRNA sites. 1 µL of DNA was used for each PCR with 12.5 µL GoTaq PCR master mix (Promega, Madison, USA), 1mM $MgCl_2$, 3% DMSO and 1 µM of each primer. Cycling parameters were 2m initial denaturation 92°C; 10 cycles 92°C 20s denaturation, 56°C 20s annealing and 68°C extension 2m; 30 cycles with 2m20s extension; 4m final elongation 68°C. PCR products were run on 2% agarose gels and sequenced by Sanger sequencing, using nested primers. PCR fragments with suspected biallelic mutations were subcloned into the vector pDONR207 by Gateway™ cloning (Invitrogen, Waltham, USA) and several colonies sequenced to assess genotype on each allele. See Appendix 2 for list of primers used.

Statistical treatment

All statistics and data visualisation were performed in GraphPad Prism 8. For Fig. 6, data were checked for homoscedasticity and normality, and ANOVA followed by Dunnet's post-hoc test, with A17 x YC3.6 as the control, were performed. Data in Fig. 7a did not meet the requirements for a parametric test and Kruskal-Wallis test was used to compare the means.

5. References

Ames, R.N., Reid, C.P.P., Porter, L.K., Cambardella, C., 1983. Hyphal Uptake and Transport of Nitrogen from Two 15N-Labelled Sources by Glomus Mosseae, a Vesicular-Arbuscular Mycorrhizal Fungus. New Phytol. 95, 381–396. https://doi.org/10.1111/j.1469-8137.1983.tb03506.x

Arazi, T., Kaplan, B., Sunkar, R., Fromm, H., 2000. Cyclic-nucleotide- and Ca2+/calmodulin-regulated channels in plants: targets for manipulating heavy-metal tolerance, and possible physiological roles. Biochem. Soc. Trans. 28, 471–475. https://doi.org/10.1042/bst0280471

Balagué, C., Lin, B., Alcon, C., Flottes, G., Malmström, S., Köhler, C., Neuhaus, G., Pelletier, G., Gaymard, F., Roby, D., 2003. HLM1, an Essential Signaling Component in the Hypersensitive Response, Is a Member of the Cyclic Nucleotide–Gated Channel Ion Channel Family. Plant Cell 15, 365–379. https://doi.org/10.1105/tpc.006999

Biel, M., 2009. Cyclic Nucleotide-regulated Cation Channels. J. Biol. Chem. 284, 9017–9021. https://doi.org/10.1074/jbc.R800075200

Brost, C., Studtrucker, T., Reimann, R., Denninger, P., Czekalla, J., Krebs, M., Fabry, B., Schumacher, K., Grossmann, G., Dietrich, P., 2019. Multiple cyclic nucleotide-gated channels coordinate calcium oscillations and polar growth of root hairs. Plant J. 99, 910–923. https://doi.org/10.1111/tpj.14371

Capoen, W., Sun, J., Wysham, D., Otegui, M.S., Venkateshwaran, M., Hirsch, S., Miwa, H., Downie, J.A., Morris, R.J., Ané, J.-M., Oldroyd, G.E.D., 2011. Nuclear membranes control symbiotic calcium signaling of legumes. Proc. Natl. Acad. Sci. 108, 14348–14353. https://doi.org/10.1073/pnas.1107912108

Carrere, S., Verdier, J., Gamas, P., 2021. MtExpress, a Comprehensive and Curated RNAseq-based Gene Expression Atlas for the Model Legume Medicago truncatula. Plant Cell Physiol. 62, 1494–1500. https://doi.org/10.1093/pcp/pcab110

Čermák, T., Curtin, S.J., Gil-Humanes, J., Čegan, R., Kono, T.J.Y., Konečná, E., Belanto, J.J., Starker, C.G., Mathre, J.W., Greenstein, R.L., Voytas, D.F., 2017. A Multipurpose Toolkit to Enable Advanced Genome Engineering in Plants. Plant Cell 29, 1196–1217. https://doi.org/10.1105/tpc.16.00922

Cervantes-Pérez, S.A., Thibivilliers, S., Laffont, C., Farmer, A.D., Frugier, F., Libault, M., 2022. Cell-specific pathways recruited for symbiotic nodulation in the Medicago truncatula legume. Mol. Plant 15, 1868–1888. https://doi.org/10.1016/j.molp.2022.10.021

Chabaud, M., Boisson-Dernier, A., Zhang, J., Taylor, C., Yu, O., Barker, D., 2006. Agrobacterium rhizogenes-Mediated Root Transformation.

Charpentier, M., 2018. Calcium signals in the plant nucleus: origin and function. J. Exp. Bot. 69, 4165–4173. https://doi.org/10.1093/jxb/ery160

Charpentier, M., Sun, J., Martins, T.V., Radhakrishnan, G.V., Findlay, K., Soumpourou, E., Thouin, J., Véry, A.-A., Sanders, D., Morris, R.J., Oldroyd, G.E.D., 2016. Nuclear-localized cyclic nucleotide–gated channels mediate

symbiotic calcium oscillations. Science 352, 1102–1105. https://doi.org/10.1126/science.aae0109

Chiasson, D.M., Haage, K., Sollweck, K., Brachmann, A., Dietrich, P., Parniske, M., 2017. A quantitative hypermorphic CNGC allele confers ectopic calcium flux and impairs cellular development. eLife 6, e25012. https://doi.org/10.7554/eLife.25012

Chin, K., DeFalco, T.A., Moeder, W., Yoshioka, K., 2013. The Arabidopsis Cyclic Nucleotide-Gated Ion Channels AtCNGC2 and AtCNGC4 Work in the Same Signaling Pathway to Regulate Pathogen Defense and Floral Transition. Plant Physiol. 163, 611–624. https://doi.org/10.1104/pp.113.225680

Choi, J., Summers, W., Paszkowski, U., 2018. Mechanisms Underlying Establishment of Arbuscular Mycorrhizal Symbioses. Annu. Rev. Phytopathol. 56, 135–160. https://doi.org/10.1146/annurev-phyto-080516-035521

Choudhury, S.R., Pandey, S., 2015. Phosphorylation-Dependent Regulation of G-Protein Cycle during Nodule Formation in Soybean. Plant Cell 27, 3260–3276. https://doi.org/10.1105/tpc.15.00517

Choudhury, S.R., Pandey, S., 2013. Specific Subunits of Heterotrimeric G Proteins Play Important Roles during Nodulation in Soybean. Plant Physiol. 162, 522–533. https://doi.org/10.1104/pp.113.215400

DeFalco, T.A., Marshall, C.B., Munro, K., Kang, H.-G., Moeder, W., Ikura, M., Snedden, W.A., Yoshioka, K., 2016. Multiple Calmodulin-Binding Sites Positively and Negatively Regulate Arabidopsis CYCLIC NUCLEOTIDE-GATED CHANNEL12. Plant Cell 28, 1738–1751. https://doi.org/10.1105/tpc.15.00870

Deguchi, Y., Banba, M., Shimoda, Y., Chechetka, S.A., Suzuri, R., Okusako, Y., Ooki, Y., Toyokura, K., Suzuki, A., Uchiumi, T., Higashi, S., Abe, M., Kouchi, H., Izui, K., Hata, S., 2007. Transcriptome Profiling of Lotus japonicus Roots During Arbuscular Mycorrhiza Development and Comparison with that of Nodulation. DNA Res. 14, 117–133. https://doi.org/10.1093/dnares/dsm014

del Cerro, P., Cook, N.M., Huisman, R., Dangeville, P., Grubb, L.E., Marchal, C., Ho Ching Lam, A., Charpentier, M., 2022. Engineered CaM2 modulates nuclear calcium oscillation and enhances legume root nodule symbiosis. Proc. Natl. Acad. Sci. 119, e2200099119. https://doi.org/10.1073/pnas.2200099119

Demidchik, V., Shabala, S., Isayenkov, S., Cuin, T.A., Pottosin, I., 2018. Calcium transport across plant membranes: mechanisms and functions. New Phytol. 220, 49–69. https://doi.org/10.1111/nph.15266

Dietrich, P., Moeder, W., Yoshioka, K., 2020. Plant Cyclic Nucleotide-Gated Channels: New Insights on Their Functions and Regulation. Plant Physiol. 184, 27–38. https://doi.org/10.1104/pp.20.00425

Ding, X.-Q., Matveev, A., Singh, A., Komori, N., Matsumoto, H., 2012. Biochemical characterization of cone cyclic nucleotide-gated (CNG) channel using the infrared fluorescence detection system. Adv. Exp. Med. Biol. 723, 769–775. https://doi.org/10.1007/978-1-4614-0631-0_98

Doudna, J.A., Charpentier, E., 2014. Genome editing. The new frontier of genome engineering with CRISPR-Cas9. Science 346, 1258096. https://doi.org/10.1126/science.1258096

Edel, K.H., Marchadier, E., Brownlee, C., Kudla, J., Hetherington, A.M., 2017. The Evolution of Calcium-Based Signalling in Plants. Curr. Biol. 27, R667–R679. https://doi.org/10.1016/j.cub.2017.05.020

Endre, G., Kereszt, A., Kevei, Z., Mihacea, S., Kaló, P., Kiss, G.B., 2002. A receptor kinase gene regulating symbiotic nodule development. Nature 417, 962–966. https://doi.org/10.1038/nature00842

Feng, C., Su, H., Bai, H., Wang, R., Liu, Y., Guo, X., Liu, C., Zhang, J., Yuan, J., Birchler, J., Han, F., 2018. High-efficiency genome editing using a dmc1 promoter-controlled CRISPR/Cas9 system in maize. Plant Biotechnol. J. 16. https://doi.org/10.1111/pbi.12920

Floss, D.S., Levy, J.G., Lévesque-Tremblay, V., Pumplin, N., Harrison, M.J., 2013. DELLA proteins regulate arbuscule formation in arbuscular mycorrhizal symbiosis. Proc. Natl. Acad. Sci. U. S. A. 110, E5025-5034. https://doi.org/10.1073/pnas.1308973110

Fonouni-Farde, C., Tan, S., Baudin, M., Brault, M., Wen, J., Mysore, K.S., Niebel, A., Frugier, F., Diet, A., 2016. DELLA-mediated gibberellin signalling regulates Nod factor signalling and rhizobial infection. Nat. Commun. 7, 12636. https://doi.org/10.1038/ncomms12636

Foyer, C.H., Lam, H.-M., Nguyen, H.T., Siddique, K.H.M., Varshney, R.K., Colmer, T.D., Cowling, W., Bramley, H., Mori, T.A., Hodgson, J.M., Cooper, J.W., Miller, A.J., Kunert, K., Vorster, J., Cullis, C., Ozga, J.A., Wahlqvist, M.L., Liang, Y., Shou, H., Shi, K., Yu, J., Fodor, N., Kaiser, B.N., Wong, F.-L., Valliyodan, B., Considine, M.J., 2016. Neglecting legumes has compromised human health and sustainable food production. Nat. Plants 2, 1–10. https://doi.org/10.1038/nplants.2016.112

Gietz, R.D., Woods, R.A., 2001. Genetic transformation of yeast. BioTechniques 30, 816–820, 822–826, 828 passim. https://doi.org/10.2144/01304rv02

Giovannetti, M., Mosse, B., 1980. An Evaluation of Techniques for Measuring Vesicular Arbuscular Mycorrhizal Infection in Roots. New Phytol. 84, 489–500. https://doi.org/10.1111/j.1469-8137.1980.tb04556.x

Govindarajulu, M., Pfeffer, P.E., Jin, H., Abubaker, J., Douds, D.D., Allen, J.W., Bücking, H., Lammers, P.J., Shachar-Hill, Y., 2005. Nitrogen transfer in the arbuscular mycorrhizal symbiosis. Nature 435, 819–823. https://doi.org/10.1038/nature03610

Harrison, M.J., 2005. Signaling in the Arbuscular Mycorrhizal Symbiosis. Annu. Rev. Microbiol. 59, 19–42. https://doi.org/10.1146/annurev.micro.58.030603.123749

Harrison, M.J., 1997. The Arbuscular Mycorrhizal Symbiosis, in: Stacey, G., Keen, N.T. (Eds.), Plant-Microbe Interactions. Springer US, Boston, MA, pp. 1–34. https://doi.org/10.1007/978-1-4615-6019-7_1

He, J., Zhang, C., Dai, H., Liu, H., Zhang, X., Yang, J., Chen, X., Zhu, Y., Wang, D., Qi, X., Li, W., Wang, Z., An, G., Yu, N., He, Z., Wang, Y.-F., Xiao, Y., Zhang, P., Wang, E., 2019. A LysM Receptor Heteromer Mediates Perception of

Arbuscular Mycorrhizal Symbiotic Signal in Rice. Mol. Plant 12, 1561–1576. https://doi.org/10.1016/j.molp.2019.10.015

Hirsch, S., Oldroyd, G.E., 2009. GRAS-domain transcription factors that regulate plant development. Plant Signal. Behav. 4, 698–700.

Hohnjec, N., Vieweg, M.F., Pühler, A., Becker, A., Küster, H., 2005. Overlaps in the Transcriptional Profiles of Medicago truncatula Roots Inoculated with Two Different Glomus Fungi Provide Insights into the Genetic Program Activated during Arbuscular Mycorrhiza. Plant Physiol. 137, 1283–1301. https://doi.org/10.1104/pp.104.056572

James, Z.M., Borst, A.J., Haitin, Y., Frenz, B., DiMaio, F., Zagotta, W.N., Veesler, D., 2017. CryoEM structure of a prokaryotic cyclic nucleotide-gated ion channel. Proc. Natl. Acad. Sci. U. S. A. 114, 4430–4435. https://doi.org/10.1073/pnas.1700248114

Jardinaud, M.-F., Fromentin, J., Auriac, M.-C., Moreau, S., Pecrix, Y., Taconnat, L., Cottret, L., Aubert, G., Balzergue, S., Burstin, J., Carrere, S., Gamas, P., 2022. MtEFD and MtEFD2: Two transcription factors with distinct neofunctionalization in symbiotic nodule development. Plant Physiol. 189, 1587–1607. https://doi.org/10.1093/plphys/kiac177

Jin, Y., Liu, H., Luo, D., Yu, N., Dong, W., Wang, C., Zhang, X., Dai, H., Yang, J., Wang, E., 2016. DELLA proteins are common components of symbiotic rhizobial and mycorrhizal signalling pathways. Nat. Commun. 7, 12433. https://doi.org/10.1038/ncomms12433

Kelner, A., Leitão, N., Chabaud, M., Charpentier, M., de Carvalho-Niebel, F., 2018. Dual Color Sensors for Simultaneous Analysis of Calcium Signal Dynamics in the Nuclear and Cytoplasmic Compartments of Plant Cells. Front. Plant Sci. 9.

Kerppola, T.K., 2006. Visualization of molecular interactions by fluorescence complementation. Nat. Rev. Mol. Cell Biol. 7, 449–456. https://doi.org/10.1038/nrm1929

Kevei, Z., Lougnon, G., Mergaert, P., Horváth, G.V., Kereszt, A., Jayaraman, D., Zaman, N., Marcel, F., Regulski, K., Kiss, G.B., Kondorosi, A., Endre, G., Kondorosi, E., Ané, J.-M., 2007. 3-hydroxy-3-methylglutaryl coenzyme a reductase 1 interacts with NORK and is crucial for nodulation in Medicago truncatula. Plant Cell 19, 3974–3989. https://doi.org/10.1105/tpc.107.053975

Lee, C.-H., MacKinnon, R., 2017. Structures of the human HCN1 hyperpolarization-activated channel. Cell 168, 111-120.e11. https://doi.org/10.1016/j.cell.2016.12.023

Leng, Q., Mercier, R.W., Hua, B.-G., Fromm, H., Berkowitz, G.A., 2002. Electrophysiological Analysis of Cloned Cyclic Nucleotide-Gated Ion Channels. Plant Physiol. 128, 400–410. https://doi.org/10.1104/pp.010832

Leng, Q., Mercier, R.W., Yao, W., Berkowitz, G.A., 1999. Cloning and First Functional Characterization of a Plant Cyclic Nucleotide-Gated Cation Channel1. Plant Physiol. 121, 753–761. https://doi.org/10.1104/pp.121.3.753

Lenzoni, G., Knight, M.R., 2019. Increases in Absolute Temperature Stimulate Free Calcium Concentration Elevations in the Chloroplast. Plant Cell Physiol. 60, 538–548. https://doi.org/10.1093/pcp/pcy227

Li, M., Zhou, X., Wang, S., Michailidis, I., Gong, Y., Su, D., Li, H., Li, X., Yang, J., 2017. Structure of a eukaryotic cyclic nucleotide-gated channel. Nature 542, 60–65. https://doi.org/10.1038/nature20819

Liang, Y., Tóth, K., Cao, Y., Tanaka, K., Espinoza, C., Stacey, G., 2014. Lipochitooligosaccharide recognition: an ancient story. New Phytol. 204, 289–296. https://doi.org/10.1111/nph.12898

Ma, Y., Garrido, K., Ali, R., Berkowitz, G.A., 2023. Phenotypes of cyclic nucleotide-gated cation channel mutants: probing the nature of native channels. Plant J. 113, 1223–1236. https://doi.org/10.1111/tpj.16106

MacLean, A.M., Bravo, A., Harrison, M.J., 2017. Plant Signaling and Metabolic Pathways Enabling Arbuscular Mycorrhizal Symbiosis. Plant Cell 29, 2319–2335. https://doi.org/10.1105/tpc.17.00555

Mair, A., Xu, S.-L., Branon, T.C., Ting, A.Y., Bergmann, D.C., 2019. Proximity labeling of protein complexes and cell-type-specific organellar proteomes in Arabidopsis enabled by TurboID. eLife 8, e47864. https://doi.org/10.7554/eLife.47864

Manthey, K., Krajinski, F., Hohnjec, N., Firnhaber, C., Pühler, A., Perlick, A.M., Küster, H., 2004. Transcriptome profiling in root nodules and arbuscular mycorrhiza identifies a collection of novel genes induced during Medicago truncatula root endosymbioses. Mol. Plant-Microbe Interact. MPMI 17, 1063–1077. https://doi.org/10.1094/MPMI.2004.17.10.1063

Mäser, P., Thomine, S., Schroeder, J.I., Ward, J.M., Hirschi, K., Sze, H., Talke, I.N., Amtmann, A., Maathuis, F.J.M., Sanders, D., Harper, J.F., Tchieu, J., Gribskov, M., Persans, M.W., Salt, D.E., Kim, S.A., Guerinot, M.L., 2001. Phylogenetic Relationships within Cation Transporter Families of Arabidopsis. Plant Physiol. 126, 1646–1667. https://doi.org/10.1104/pp.126.4.1646

McAinsh, M.R., Pittman, J.K., 2009. Shaping the calcium signature. New Phytol. 181, 275–294. https://doi.org/10.1111/j.1469-8137.2008.02682.x

Meena, M.K., Prajapati, R., Krishna, D., Divakaran, K., Pandey, Y., Reichelt, M., Mathew, M.K., Boland, W., Mithöfer, A., Vadassery, J., 2019. The Ca2+ Channel CNGC19 Regulates Arabidopsis Defense Against Spodoptera Herbivory. Plant Cell 31, 1539–1562. https://doi.org/10.1105/tpc.19.00057

Meng, Y., Hou, Y., Wang, H., Ji, R., Liu, B., Wen, J., Niu, L., Lin, H., 2017. Targeted mutagenesis by CRISPR/Cas9 system in the model legume Medicago truncatula. Plant Cell Rep. 36, 371–374. https://doi.org/10.1007/s00299-016-2069-9

Miransari, M., 2010. Contribution of arbuscular mycorrhizal symbiosis to plant growth under different types of soil stress. Plant Biol. 12, 563–569. https://doi.org/10.1111/j.1438-8677.2009.00308.x

Nanjareddy, K., Arthikala, M.-K., Gómez, B.-M., Blanco, L., Lara, M., 2017. Differentially expressed genes in mycorrhized and nodulated roots of common bean are associated with defense, cell wall architecture, N metabolism, and P metabolism. PLOS ONE 12, e0182328. https://doi.org/10.1371/journal.pone.0182328

Oldroyd, G.E.D., Murray, J.D., Poole, P.S., Downie, J.A., 2011. The Rules of Engagement in the Legume-Rhizobial Symbiosis. Annu. Rev. Genet. 45, 119–144. https://doi.org/10.1146/annurev-genet-110410-132549

Osman, A., 2004. Yeast two-hybrid assay for studying protein-protein interactions. Methods Mol. Biol. Clifton NJ 270, 403–422. https://doi.org/10.1385/1-59259-793-9:403

Pan, Y., Chai, X., Gao, Q., Zhou, L., Zhang, S., Li, L., Luan, S., 2019. Dynamic Interactions of Plant CNGC Subunits and Calmodulins Drive Oscillatory Ca2+ Channel Activities. Dev. Cell 48, 710-725.e5. https://doi.org/10.1016/j.devcel.2018.12.025

Pecrix, Y., Sallet, E., Moreau, S., Bouchez, O., Carrere, S., Gouzy, J., Jardinaud, M.-F., Gamas, P., 2022. DNA demethylation and hypermethylation are both required for late nodule development in Medicago. Nat. Plants 8, 741–749. https://doi.org/10.1038/s41477-022-01188-w

Roux, B., Rodde, N., Jardinaud, M.-F., Timmers, T., Sauviac, L., Cottret, L., Carrère, S., Sallet, E., Courcelle, E., Moreau, S., Debellé, F., Capela, D., de Carvalho-Niebel, F., Gouzy, J., Bruand, C., Gamas, P., 2014. An integrated analysis of plant and bacterial gene expression in symbiotic root nodules using laser-capture microdissection coupled to RNA sequencing. Plant J. 77, 817–837. https://doi.org/10.1111/tpj.12442

Sakamoto, K., Ogiwara, N., Kaji, T., Sugimoto, Y., Ueno, M., Sonoda, M., Matsui, A., Ishida, J., Tanaka, M., Totoki, Y., Shinozaki, K., Seki, M., 2019. Transcriptome analysis of soybean (Glycine max) root genes differentially expressed in rhizobial, arbuscular mycorrhizal, and dual symbiosis. J. Plant Res. 132, 541–568. https://doi.org/10.1007/s10265-019-01117-7

Shuart, N.G., Haitin, Y., Camp, S.S., Black, K.D., Zagotta, W.N., 2011. Molecular mechanism for 3:1 subunit stoichiometry of rod cyclic nucleotide-gated ion channels. Nat. Commun. 2, 457. https://doi.org/10.1038/ncomms1466

Sieberer, B.J., Chabaud, M., Fournier, J., Timmers, A.C.J., Barker, D.G., 2012. A switch in Ca2+ spiking signature is concomitant with endosymbiotic microbe entry into cortical root cells of Medicago truncatula. Plant J. 69, 822–830. https://doi.org/10.1111/j.1365-313X.2011.04834.x

Soltis, D.E., Soltis, P.S., Morgan, D.R., Swensen, S.M., Mullin, B.C., Dowd, J.M., Martin, P.G., 1995. Chloroplast gene sequence data suggest a single origin of the predisposition for symbiotic nitrogen fixation in angiosperms. Proc. Natl. Acad. Sci. U. S. A. 92, 2647–2651.

Stracke, S., Kistner, C., Yoshida, S., Mulder, L., Sato, S., Kaneko, T., Tabata, S., Sandal, N., Stougaard, J., Szczyglowski, K., Parniske, M., 2002. A plant receptor-like kinase required for both bacterial and fungal symbiosis. Nature 417, 959–962. https://doi.org/10.1038/nature00841

Tan, Y.-Q., Yang, Y., Shen, X., Zhu, M., Shen, J., Zhang, W., Hu, H., Wang, Y.-F., 2023. Multiple cyclic nucleotide-gated channels function as ABA-activated Ca2+ channels required for ABA-induced stomatal closure in Arabidopsis. Plant Cell 35, 239–259. https://doi.org/10.1093/plcell/koac274

Tian, W., Hou, C., Ren, Z., Wang, C., Zhao, F., Dahlbeck, D., Hu, S., Zhang, L., Niu, Q., Li, L., Staskawicz, B.J., Luan, S., 2019. A calmodulin-gated calcium channel links pathogen patterns to plant immunity. Nature 572, 131–135. https://doi.org/10.1038/s41586-019-1413-y

Tromas, A., Parizot, B., Diagne, N., Champion, A., Hocher, V., Cissoko, M., Crabos, A., Prodjinoto, H., Lahouze, B., Bogusz, D., Laplaze, L., Svistoonoff, S., 2012. Heart of Endosymbioses: Transcriptomics Reveals a Conserved Genetic Program among Arbuscular Mycorrhizal, Actinorhizal and Legume-Rhizobial Symbioses. PLOS ONE 7, e44742. https://doi.org/10.1371/journal.pone.0044742

Venkateshwaran, M., Jayaraman, D., Chabaud, M., Genre, A., Balloon, A.J., Maeda, J., Forshey, K., den Os, D., Kwiecien, N.W., Coon, J.J., Barker, D.G., Ané, J.-M., 2015. A role for the mevalonate pathway in early plant symbiotic signaling. Proc. Natl. Acad. Sci. 112, 9781–9786. https://doi.org/10.1073/pnas.1413762112

Weitz, D., Ficek, N., Kremmer, E., Bauer, P.J., Kaupp, U.B., 2002. Subunit stoichiometry of the CNG channel of rod photoreceptors. Neuron 36, 881–889. https://doi.org/10.1016/s0896-6273(02)01098-x

Xue, J., Han, Y., Zeng, W., Jiang, Y., 2022. Structural mechanisms of assembly, permeation, gating, and pharmacology of native human rod CNG channel. Neuron 110, 86-95.e5. https://doi.org/10.1016/j.neuron.2021.10.006

Zeb, Q., Wang, X., Hou, C., Zhang, X., Dong, M., Zhang, S., Zhang, Q., Ren, Z., Tian, W., Zhu, H., Li, L., Liu, L., 2020. The interaction of CaM7 and CNGC14 regulates root hair growth in Arabidopsis. J. Integr. Plant Biol. 62, 887–896. https://doi.org/10.1111/jipb.12890

Zhang, X., Dong, W., Sun, J., Feng, F., Deng, Y., He, Z., Oldroyd, G.E.D., Wang, E., 2015. The receptor kinase CERK1 has dual functions in symbiosis and immunity signalling. Plant J. 81, 258–267. https://doi.org/10.1111/tpj.12723

Zhang, Z., Hou, C., Tian, W., Li, L., Zhu, H., 2019. Electrophysiological Studies Revealed CaM1-Mediated Regulation of the Arabidopsis Calcium Channel CNGC12. Front. Plant Sci. 10.

Zhong, H., Molday, L.L., Molday, R.S., Yau, K.-W., 2002. The heteromeric cyclic nucleotide-gated channel adopts a 3A:1B stoichiometry. Nature 420, 193–198. https://doi.org/10.1038/nature01201

Zhu, F., Ye, Q., Chen, H., Dong, J., Wang, T., 2021. Multigene editing reveals that MtCEP1/2/12 redundantly control lateral root and nodule number in Medicago truncatula. J. Exp. Bot. 72, 3661–3676. https://doi.org/10.1093/jxb/erab093

6. Appendix

Appendix 1. List of constructs used.

Table 1.1. List of constructs made by Gateway assembly.

Description	Vector	Insert	Relevant section	Acknowledgement
Subclone CNGCD promoter	pDONR207	pCNGCD	2.1 (Fig. 1)	N Cook
Fuse CNGCD promoter to GUS	pKGW-RR-GUS	pCNGCD	2.1 (Fig. 1)	N Cook
Subclone CNGCD N terminus	pDONR207	CNGCD Nt	2.2 (Fig. 5)	P Del Cerro
Fuse CNGCD to AD	pAD	CNGCD Nt	2.2 (Fig. 5)	P Del Cerro
Fuse CNGCD to BD	pBD	CNGCD Nt	2.2 (Fig. 5)	P Del Cerro
Subclone DMI1 C terminus	pDONR207	DMI1 Ct	2.2 (Fig. 5)	M Charpentier
Fuse DMI1 to AD	pAD	DMI1 Ct	2.2 (Fig. 5)	M Charpentier
Fuse DMI1 to BD	pBD	DMI1 Ct	2.2 (Fig. 5)	M Charpentier

Table 1.2. List of constructs made by Golden Gate assembly.

Description	Level	Vector	Inserts	Relevant section	Acknowledgement
pCNGC15a:GUS	L2	EC50507	35s:DsRed_pCNGC15a:GUS_linker	2.1 (Figure 1)	M Charpentier
pCNGC15b:GUS	L2	EC50507	35s:DsRed_pCNGC15b:GUS_linker	2.1 (Figure 1)	M Charpentier
pCNGC15c:GUS	L2	EC50507	35s:DsRed_pCNGC15c:GUS_linker	2.1 (Figure 1)	M Charpentier
VenusN:CNGCD	L1	EC47802 R1	pLjUB_VenusN_CNGCD_t35s	2.2 (Figs 2-4)	R Huisman
VenusN:CNGC15a	L1	EC47802 R1	pLjUB_VenusN_CNGC15a_t35s	2.2 (Figs 2-4)	M Charpentier
VenusN:CNGC15b	L1	EC47802 R1	pLjUB_VenusN_CNGC15b_t35s	2.2 (Figs 2-4)	M Charpentier
VenusN:CNGC15c	L1	EC47802 R1	pLjUB_VenusN_CNGC15c_t35s	2.2 (Figs 2-4)	M Charpentier
VenusC:CNGCD	L1	EC47811 R2	pNOS_VenusC_CNGCD_tNOS	2.2 (Figs 2-4)	R Huisman
VenusC:CNGC15a	L1	EC47811 R2	pNOS_VenusC_CNGC15a_tNOS	2.2 (Figs 2-4)	M Charpentier
VenusC:CNGC15b	L1	EC47811 R2	pNOS_VenusC_CNGC15b_tNOS	2.2 (Figs 2-4)	M Charpentier
VenusC:CNGC15c	L1	EC47811 R2	pNOS_VenusC_CNGC15c_tNOS	2.2 (Figs 2-4)	M Charpentier
DMI1:VenusC	L1	EC47811 R2	pNOS_DMI1_VenusC_tNOS	2.2 (Figs 2-4)	M Charpentier
CNGCD:VenusN	L1	EC47802 R1	pLjUB_CNGCD_VenusN_t35s	2.2 (Figs 2-4)	R Huisman
CNGCD:VenusC	L1	EC47811 R2	pNOS_CNGCD_VenusC_tNOS	2.2 (Figs 2-4)	R Huisman
15a/D Nterm	L2	EC50507	VenusN:CNGC15a_VenusC:CNGCD_mCherry_KanR_linker	2.2 (Figs 2,4)	R Huisman
15b/D Nterm	L2	EC50507	VenusN:CNGC15b_VenusC:CNGCD_mCherry_KanR_linker	2.2 (Figs 2,4)	R Huisman
15c/D Nterm	L2	EC50507	VenusN:CNGC15c_VenusC:CNGCD_mCherry_KanR_linker	2.2 (Figs 2,4)	R Huisman
D Nterm/DMI1 Cterm	L2	EC50507	VenusN:CNGCD_DMI1:VenusC_mCherry_KanR_linker	2.2 (Figs 2,4)	R Huisman
D/D Nterm	L2	EC50507	VenusN:CNGCD_VenusC:CNGCD_mCherry_KanR_linker	2.2 (Figs 3,4)	R Huisman
D/D Cterm	L2	EC50507	CNGCD:VenusN_CNGCD:VenusC_mCherry_KanR_linker	2.2 (Figs 3,4)	R Huisman
15a/15a Nterm	L2	EC50507	VenusN:CNGC15a_VenusC:CNGC15a_mCherry_KanR_linker	2.2 (Figs 3,4)	R Huisman
15b/15b Nterm	L2	EC50507	VenusN:CNGC15b_VenusC:CNGC15b_mCherry_KanR_linker	2.2 (Figs 3,4)	R Huisman
15c/15c Nterm	L2	EC50507	VenusN:CNGC15c_VenusC:CNGC15c_mCherry_KanR_linker	2.2 (Figs 3,4)	R Huisman

CNGCD sgRNA 1	L1	EC47751 F3	pMtU6_gRNA1	2.3.2 (Fig 7)	R Huisman
CNGCD sgRNA 3	L1	EC47761 F4	pMtU6_gRNA3	2.3.2 (Fig 7)	R Huisman
CNGCD sgRNA 2	L1	EC47772 F5	pMtU6_gRNA2	2.3.2 (Fig 7)	R Huisman
CNGCD-CRISPR	L2	EC50507	mCherry_Cas9_guide1_guide3_guide2_linker	2.3.2 (Fig 7)	R Huisman
EV-Free Cas9	L2	EC50507	mCherry_Cas9_linker	2.3.2 (Fig 7)	R Huisman
CNGCD-CRISPR (stable mutant line)	L2	EC50507	RUBY_Cas9_guide1_guide3_linker	2.3.3	N Cook

Appendix 2. List of primers used.

Primer description	Sequence	Relevant section
Genotyping PCR CNGCD-CRISPR F	GCCGACATTCACTAACATGTTC	2.3.2-3
Genotyping PCR CNGCD-CRISPR R	GTCTCAACCTCTGTTAACGCCT	2.3.2-3
Sequencing CNGCD-CRISPR	GTTCTGATGTACTAGCAACAAAGC	2.3.2-3
Sequencing CNGCD-CRISPR	TCGAACTTGATCCCTCTGGT	2.3.2-3
Sequencing CNGCD-CRISPR	AGATCCCTCATGTGACATCC	2.3.2-3
Subcloning CNGCD-CRISPR PCR products for sequencing	GGGGACAAGTTTGTACAAAAAAGCAGGCTTCGCCGACATTCACTAACATGTTC	2.3.2-3
Subcloning CNGCD-CRISPR PCR products for sequencing	GGGGACCACTTTGTACAAGAAAGCTGGGTGGTCTCAACCTCTGTTAACGCCT	2.3.2-3